Published in final edited form as:
Biochim Biophys Acta. 2013 October ; 1830(10): 4692–4707. doi:10.1016/j.bbagen.2013.05.033.

Kinetics of extracellular ATP in mastoparan 7-activated human erythrocytes

María Florencia Leal Denis[a], **J. Jeremías Incicco**[a], **María Victoria Espelt**[a], **Sandra V. Verstraeten**[a], **Omar P. Pignataro**[b,c], **Eduardo R. Lazarowski**[d], and **Pablo J. Schwarzbaum**[a,*]

[a]IQUIFIB, Department of Biological Chemistry, School of Pharmacy and Biochemistry, University of Buenos Aires, Buenos Aires, Argentina

[b]Laboratory of Molecular Endocrinology and Signal Transduction, Institute of Biology and Experimental Medicine-CONICET, Vuelta de Obligado 2490, CP 1428 Buenos Aires, Argentina

[c]Department of Biological Chemistry. School of Sciences. University of Buenos Aires, Buenos Aires, Argentina

[d]Cystic Fibrosis/Pulmonary Research and Treatment Center, University of North Carolina at Chapel Hill, 4029A Thurston Bowles Building, Chapel Hill, NC 27599-7248, USA

SUMMARY

Background—The peptide mastoparan 7 (MST7) stimulated ATP release in human erythrocytes. We explored intra- and extracellular processes governing the time-dependent accumulation of extracellular ATP (i.e., ATPe kinetics).

Methods—Human erythrocytes were treated with MST7 in the presence or absence of two blockers of pannexin 1. ATPe concentration was monitored by luciferin-luciferase based real-time luminometry.

Results—Exposure of human erythrocytes to MST7 led to an acute increase in [ATPe], followed by a slower increase phase. ATPe kinetics reflected a strong activation of ATP efflux and a low rate of ATPe hydrolysis by ectoATPase activity. Enhancement of [ATPe] by MST7 required adhesion of erythrocytes to poly-D-lysin-coated coverslips, and correlated with a 31% increase of cAMP and 10% cell swelling. However, when MST7 was dissolved in a hyperosmotic medium to block cell swelling, ATPe accumulation was inhibited by 49%. Erythrocytes pre-exposure to 10 μM of either carbenoxolone or probenecid, two blockers of pannexin 1, exhibited a partial reduction of ATP efflux. Erythrocytes from pannexin 1 knockout mice exhibited similar ATPe kinetics as those of wild type mice erythrocytes exposed to pannexin 1 blockers.

Conclusions—MST7 induced release of ATP required either cell adhesion or strong activation of cAMP synthesis. Part of this release required cell swelling. Kinetic analysis and a data driven model suggested that ATP efflux is mediated by two ATP conduits displaying different kinetics, with one conduit being fully blocked by pannexin 1 blockers.

[*]Address correspondence to: Dr. Pablo J. Schwarzbaum. IQUIFIB, Facultad de Farmacia y Bioquímica, UBA. Junín 956, C1113AAD, Buenos Aires, Argentina. Fax (5411) 4 962 5457; Tel (5411) 4 964 8289/90/91 ext. 128; pjs@qb.ffyb.uba.ar.

General Significance—Kinetic analysis of extracellular ATP accumulation from human erythrocytes and potential effects on microcirculation.

Keywords

Extracellular ATP; ATPases; Erythrocyte; Pannexin 1

1. INTRODUCTION

In healthy humans, about 40% of the blood volume is occupied by rbcs containing a 1,000-fold higher ATP concentration than plasma (mM vs μM; (1)). Thus even a limited release of ATP from the large rbc intracellular pool can result in nano to micromolar concentrations of ATP (ATPe) in the vascular lumen [1, 2, 3].

Human erythrocytes release ATP upon their exposure to β-adrenergic agonists, mechanical deformation, reduced oxygen tension, or acidosis [4]. All of these conditions represent physiological stimuli to which rbcs are exposed in the vasculature, *e.g.* when passing through the small branches of the microcirculation [5, 6, 7, 8].

A signaling route leading to ATP release from human rbcs involves the heterotrimeric G protein Gs, adenylyl cyclases and PKA [3, 9]. In addition to Gs, Gi proteins of these cells have been proposed to transduce mechanical stress and hypoxia into ATP release [10, 11].

Similarly, the tetradecapeptide MST extracted from wasp venom [12] binds to the plasma membrane and forms an amphiphilic helix that activates Gi without requiring the activation of a receptor [13]. MST7, synthesized by substituting alanine for the positively charged lysine in position 12, acts as a potent analog of MST in human rbcs and other cell systems [14,15]. Both MST and MST7 are known to activate ATP efflux of human rbcs [15].

The current postulated chain of events linking Gi activation to ATP efflux involves the dissociation of heterotrimeric Gi, allowing βγ dimers to stimulate specific isoforms of adenylyl cyclases, and the subsequent increase in cAMP formation. These events are followed by a series of not-well defined intracellular signaling events upstream of ATP release [10, 11, 16]. Besides the adenylyl cyclases, βγ subunits interact with various effector proteins such as ionic channels, phosphatidylinositol-3 kinase isoforms, proteins containing PDZ domains, and GEFs for small G proteins [17].

The released ATP can primarily act on specific P2X and P2Y purinergic receptors (receptors for di- and trinucleotides, [2]) on adjacent endothelial cells, or be hydrolyzed by ectonucleotidases present on the plasma membrane of rbcs and other blood and vascular cells. Thus ATPe also serves as a reservoir to generate ADP and adenosine, which in turn activate P2Y and adenosine receptors functionally expressed in rbcs [18, 19] and endothelial cells [20, 21, 22]. The physiological effects of such ligand-receptor interactions can be manifold, including the alteration of the vascular tone in the brain, coronary arteries and skeletal muscle [23, 24].

Despite the accumulated knowledge on the mechanisms mediating ATP release, purinergic receptor signaling, and the cellular role of various ectonucleotidases [25], little is known

regarding how the dynamic interaction of these processes controls the kinetics of ATPe accumulation in the immediate environment of rbcs. This is particularly important in the microvasculature, where rbcs and other blood cells interact over short distances (within the micrometer range), and local signals of high energy demand and/or stress can induce ATP release from erythrocytes. The subsequent extracellular diffusion would permit ATPe to trigger paracrine responses to these signals. Based on this, the following questions arise: (i) will ATP release, under a given metabolic condition, be counteracted by ATPe hydrolysis at the cell surface? This is not unexpected since in most cell types ectoATPase activity follows a function with [ATPe] [26], (ii) can the released ATP, as part of a postulated negative feedback system [27, 28], inhibit one or more components that participate in ATP release? and (iii) what ATP transport mechanisms operate in rbcs?

The non-nucleated human rbcs offer a simple metabolic model to approach these questions, because they possess glycolysis as the sole pathway for ATP generation and lack intracellular compartments, so that no exocytotic ATP release can occur in these cells. Moreover, these cells lack direct cell-cell communication that might increase the available signaling mechanisms inducing ATP release, which may complicate the analysis of ATPe regulation. Still, the kinetics of [ATPe] in the rbc model, as in any other cell, is complex enough due to the non-linear relationships among the different processes that alter ATPe concentration. For instance, various channels and transporters have been postulated in human rbcs as candidates for ATP release, although many of them have been rejected afterwards as main conduits [29].

In mammals, the prime candidate protein mediating conductive ATP release is the pannexon, a homohexamer of pannexin 1, which is expressed in rbcs [27]. The pannexon constitutes a large pore by itself or it can be part of a multiprotein complex capable of carrying anions and signaling molecules from the cytoplasm to the extracellular space [30].

Since MST7 is a robust activator of rbcs ATP release [31, 32, 33], in this study we intended to understand the kinetics of ATPe by exposing human erythrocytes to this peptide.

We present experimental evidence showing that several potential factors altering the kinetics of [ATPe] can be experimentally controlled in a way that allows a quantitative description of ATP transmembrane fluxes, and provides useful information on the underlying mechanisms enabling such transport.

By fitting a simple mathematical model to the experimental ATPe kinetics of erythrocytes, and from the analysis of ATP release of rbcs from human, canine and mice ($pnx^{+/+}$ and $pnx^{-/-}$) we demonstrate the existence of two kinetically different ATP pathways mediating ATP release.

2. MATERIALS AND METHODS

2.1. Chemicals

All reagents in this study were of analytical grade. Mastoparan 7, mastoparan 17, carbenoxolone, probenecid, firefly luciferase (EC 1.13.12.7), forskolin, isoproterenol, papaverine, H-89, laminin and collagen were purchased from Sigma-Aldrich (St. Louis,

MO, USA). BCECF-AM, Fluo 4-AM and D-luciferin were obtained from Invitrogen/ Molecular Probes Inc. (Eugene, OR, USA). [γ-^{32}P]ATP (10 Ci/mmol) was purchased from Perkin Elmer Life Sciences (Santa Clara, California, USA).

2.2. Isolation of erythrocytes

Human rbcs were isolated as described before [3]. Before the experiments, rbcs were resuspended in RBC medium containing (in mM) 137 NaCl, 2.7 KCl, 4.72 Na_2HPO_4, 1.50 KH_2PO_4, 1.32 $CaCl_2$, 1.91 $MgSO_4$, 5 glucose, 0.5% bovine serum albumin, pH 7.4 at 25ºC, and 300 mOsm. All procedures conformed to the Declaration of Helsinki and written informed consent was given by the donors. Erythrocytes from dogs and mice were isolated similarly to human rbcs.

2.3. Pannexin 1 knockout mice

The pannexin 1 knockout mouse was generated and characterized, as previously described [34]. Heterozygous mice were bred to produce homozygous pannexin 1 deficient animals. All animal studies were approved by the Institutional Animal Care and Use Committee and were performed according to principles outlined by the Animal Welfare and the NIH guidelines for the care and use of animals in biomedical research. No morphological differences or cell volume variation were observed between wild type and pannexin 1 knockout mice rbcs through microscopy, hematocrit and cell counting techniques.

2.4. Treatments

ATP release was induced with 10 μM MST7 or a mixture called 3V, which contained 10 μM isoproterenol, 30 μM forskolin and 100 μM papaverin [3]. Carbenoxolone 10 M or 100 μM and probenecid 10 μM were used as blockers of ATP release. H-89 10 μM was used as a PKA inhibitor.

2.5. Extracellular and intracellular ATP measurements

ATPe was measured using firefly luciferase, which catalyzes the oxidation of luciferin in the presence of ATP to produce light [35; 36]. Two different types of luminometry determinations were performed, *real-time* and *off-line*.

Real-time luminometry measurements were carried out with cells laid on coverslips that were mounted in the assay chamber of a custom-built luminometer, as previously described [37]. Because luciferase activity at 37 ºC is only 10% of that observed at 20 ºC [38], to maintain full luciferase activity, ATP measurements were performed in a cool chamber acclimated at 20 ºC. Under the experimental conditions, assay volume did not change during the course of the experiment. Most measurements were performed with $3x10^6$ cells incubated in 40 μl of RBC medium. Under these conditions the medium has a height of about 104 μm (height at the coverslip bottom of the chamber equals 0). The time course of light emission was transformed into ATPe concentration *versus* time by means of a calibration curve. Increasing concentrations of ATP from 9 to 3,900 nM were sequentially added to the assay medium from a stock solution of pure ATP dissolved in RBC medium.

In the real-time technique ATPe was measured using cells attached to coated coverslips (denoted as adhered cells), or cells loaded on the coverslip surface in the absence of any adherent substrate (non-adhered cells). For adhered cells, rbcs were attached on coverslips coated with 0.001% poly-D-lysine, except in experiments of Suppl. Fig. 3, where coverslips were coated with 5 μg laminin or with 0.5–5–50 μg collagen.

Results were expressed as [ATPe] at every time point of a kinetic curve (i.e., ATPe kinetics), with [ATPe] expressed as pmol/10^6 cells or nM/40 μl. Alternatively, increases in [ATPe] were evaluated as the difference between [ATPe] at a fixed time point post stimulus and the basal [ATPe], and are indicated as ΔATP_{20} (20 min post stimulus, for human rbcs) or ΔATP_5 (5 min post stimulus, for mice rbcs).

For *off-line* luminometry determinations, suspensions of human rbcs were incubated in the presence of MST7. Afterwards the rbcs suspension was centrifuged 2 min at 1,000 x g. ATPe levels were determined in 45 μl of the resulting supernatant. A standard ATP curve was obtained for each experiment. Results are indicated as ΔATP_{10} which results from subtracting [ATPe] basal values to [ATPe] at 10 min post stimulus.

The intracellular content of ATP was estimated in real-time measurements, using adhered erythrocytes (3x10^6 cells). Following rbcs permeabilization with digitonin (50 μg/mL), the released cytosolic ATP was measured by luminometry as described for ATPe. After considering the total volume occupied by all rbcs present in the chamber, and the relative solvent cell volume [39], ATP values were expressed as the intracellular ATP concentration of rbcs. Changes in cell volume induced by MST7 were taken into account.

2.6. Kinetics of cytosolic free calcium (Ca^{2+}_i)

Human rbcs (3x10^6 cells) were attached to 0.001% poly-D-lysine-coated coverslips. Rbcs were incubated in RBC medium containing 5 μM Fluo-4 AM for 1 hour at 37 °C. Subsequently, the solution was washed three times with RBC medium at room temperature to eliminate extracellular Fluo-4, and coverslips were mounted on a measuring chamber of an inverted Nikon TE-200 epifluorescence microscope. Fluorescence intensity was determined at 0.5 min intervals (λexcitation 495 nm, λemission: 510 nm). Images were acquired with a charge-coupled device camera (Hamamatsu C4742-95) and the Metafluor acquisition program (Universal Imaging).

All measurements were made at 20°C. Cells were incubated in the absence and presence of MST7. After each experiment, minimal fluorescence intensity (F_{min}) was obtained by addition of 0.5 mM EGTA in a Ca^{2+} free medium. Maximal fluorescence intensity (F_{max}) was obtained after addition of 2 mM $CaCl_2$. Both measurements were performed in the presence of 10 μM of the calcium ionophore ionomycin and used to calibrate the acquired data. Results were transformed into Ca^{2+}i concentrations by using the following equation

$$[Ca_i^{2+}] = K_d \cdot \left(\frac{F - F_{min}}{F_{max} - F} \right)$$

with a dissociation constant (Kd) of 345 nM [40]. F represents the intensity of fluorescence at each time. Results were corrected considering the observed changes in cell volume induced by MST7 (see “Cell volume” below).

2.7. Hydrolysis of ATPe

The rate of ATPe hydrolysis was determined by following the accumulation of [^{32}P]Pi release from exogenous [γ-^{32}P]ATP added to a rbcs suspension of known hematocrit, as described before [41; 3] and by real-time luminometry. Briefly, in the first technique the reaction was started by adding [γ-^{32}P]ATP (0.27Ci/mmol; from 150 to 900 nM) to cell suspensions at room temperature. At different times, a 200 μL aliquot of the suspension was withdrawn and centrifuged at 900xg during 30 s, and 100 μL of the supernatant were poured into 750 μL of a stop solution containing 4.05 mM $(NH_4)_6Mo_7O_{24}$ and 0.83 mM $HClO_4$. The ammonium molybdate solution formed a complex with the released phosphate, which was then extracted with 0.6 mL of isobutyl alcohol. Phases were separated by centrifugation at 1,000xg for 5 min, aliquots of 200 μL of the organic phase containing [^{32}P]Pi were transferred to vials with 2 mL of 0.5 M NaOH and radioactivity was measured by the Cerenkov effect. Initial [^{32}P]Pi concentrations were measured in assay medium lacking cells. Because the uptake of ATP by rbcs is extremely low, any hydrolysis of [γ-^{32}P]ATP into ADP + [^{32}P]Pi in a cell suspension can be defined as ecto-ATPase activity, the time course of which yields a measure of the rate at which one or more ectonucleotidases hydrolyse ATPe. To calculate ectoATPase activity, time dependent levels of P_i were fitted to

$$Y = Y_0 + A \cdot (1 - exp^{-k \cdot t})$$

where Y and Y_0 are the values of [$^{32}P_i$] at each time (t) and at t=0, respectively; A represents the maximal value for the increase in Y with time and *k* is a rate coefficient. The parameters of best fit resulting from the regression were used to calculate the initial rate of ectoATPase activity (vi) as *k* x A (*i.e.* the first derivative of Equation 1 evaluated at t = 0). The [$^{32}P_i$] mass produced from [γ-^{32}P]ATP was calculated using the ATP specific activity.

To determine ectoATPase activity by real-time luminometry, coverslips with cells suspension (3 x 10^6 cells or 30 x 10^6 cells) were mounted in the measuring chamber of the luminometer and exposed to luciferase reaction mix. Light emission was measured for 20 min, and then ATP was added to the chamber at final concentrations of 103, 206 and 326 and 863 nM (in separate experiments), and light emission was recorded for another 20 min. Recorded light output was transformed into ATPe concentration vs. time by means of a calibration curve and the initial rate of disappearance of ATPe (vi) was estimated from ATPe kinetics.

For both the radioactive and the luminiscence method, ectoATPase activity was expressed as fmol Pi/10^6 cells/min.

2.8. Hemolysis measurements

An enzymatic method was used to detect microquantities of free hemoglobin [42]. Under the experimental conditions, as little as 0.006% hemolysis can be detected. Experiments with detectable free hemoglobin were discarded to avoid the contribution of ATPe content by hemolysis.

The methods used to measure cyclic AMP and the kinetics of cell volume from human erythrocytes have been described before [19, 3].

2.9. Data analysis

Statistical significance was determined using one-way analysis of variance followed by a Turkey-Kramer test of multiple comparisons. A p value ‹ 0.05 was considered significant. Numbers of determinations (n) from independent preparations (N) are indicated. For experiments on the time course of both, *Vr* and Ca^{2+}_i, 20–30 cells from 4 or 5 independent preparations were used.

3. RESULTS

3.1. Effect of hematocrit on [ATPe] of MST7-exposed human rbcs

Determinations of [ATPe] were performed by off-line luminometry at a fixed time point (Suppl. Fig. 1). The response of human rbcs suspensions to a 10 min MST7 exposure (ΔATP_{10}) was examined at different hematocrit values ranging from 0.075 to 20%. Results showed an increase of ΔATP_{10} with hematocrits in the higher range, since e.g. at hematocrits 5% and 20% the [ATPe] increased 4- and 17-folds the basal values, respectively. In the 0.75% and 0.075% range of hematocrit no significant changes in ΔATP_{10} were observed.

Subsequent experiments were performed using the real-time luminometry protocol for [ATPe] determination.

3.2. ATPe kinetics of MST7 exposed human rbcs

In Fig. 1 a quantification of the time dependent accumulation of ATPe is shown, and denoted as ATPe kinetics, which depends on the rates of ATP release (increasing [ATPe]) and extracellular ATP hydrolysis (decreasing [ATPe]).

In unstimulated human rbcs, both in the absence or presence of cell adhesion to poly-D-lysine coated coverslips, [ATPe] remained steady at 0.50 ± 0.11 pmoles/10^6 cells. In non-adhered human rbcs MST7 did not affect [ATPe] (Fig. 1A). Lack of response to MST7 was also evident when non-adhered cells where co-incubated in the presence of soluble lysine (67 mg/mL) or soluble poly-D-lysine (0.01 mg/mL) (Fig. 1B).

However, in cells attached to poly-D-lysine coated coverslips, MST7 promoted an acute, 7-fold increase in [ATPe] followed by a slower increase phase, with [ATPe] amounting to 3.41 ± 0.25 pmoles·/10^6 cells at 20 min post-stimulus (Fig. 1A). ATPe kinetics was well described by the sum of two increasing exponential functions of time: a fast phase spanning about 70% of total [ATPe] change with $t_{1/2}$ = 0.146 ± 0.003 min and a slow phase with $t_{1/2}$

= 6.1 ± 0.1 min. In similar experiments using more prolonged MST7 exposures, [ATPe] achieved a steady state value (Suppl. Fig. 2).

Exposure of adhered cells to MST17, an inactive analogue of MST7, was not different from basal values. Pretreatment of rbcs with PTX, which uncoupled Gi/o from their effectors, inhibited MST7-induced ATPe accumulation by 89% ([ATPe] = 0.85 ± 0.12 pmoles/10^6 cells after 20 min) (Fig. 1C).

In separate experiments, release of ATP was also observed when cells were attached to either laminin- or collagen- coated coverslips (Suppl. Fig. 3).

3.3. Effect of cell volume on ATPe kinetics of MST7 exposed human rbcs

Changes in the volume of rbcs may alter signaling mechanisms leading to ATP efflux, with concomitant changes in ATPe kinetics. Therefore the possibility that cell volume may be affected by MST7 exposure was investigated.

When challenged with 10 μM MST7 in RBC isosmotic medium, cells swelled acutely by 10 % (Vr= 1.10 ± 0.01; N=8). The time course of Vr changes was well described by the sum of two increasing exponential functions of time (Fig. 2A): a fast phase spanning about 50% of total Vr change with $t_{1/2}$ value of 0.04 min and a slow phase with $t_{1/2}$ = 5 ± 2 min.

Since a slight hyposmotic treatment (in the absence of MST7) induced a small swelling and [ATPe] increase (Suppl. Fig. 4), the relationship between MST7 effect on ATPe kinetics and on the observed changes in cell volume was evaluated.

To this end, MST7 was prepared in a hyperosmotic medium (345 mosM) to fully block cell swelling (Fig. 2A). Under this condition ATPe accumulation was partially inhibited (Fig. 2B) with respect to that observed in isosmotic medium.

In hyperosmotic medium ATPe kinetics was well described by the sum of two exponential functions of time with similar $t_{1/2}$ values as those observed with MST7 in isosmotic medium: a fast phase with $t_{1/2}$ = 0.23 ± 0.01 min and a slow phase with $t_{1/2}$ = 5.4 ± 0.2 min.

3.4. Intracellular signaling

To investigate second messengers mediating ATP release, the effect of MST7 on the concentrations of cytosolic cAMP and calcium ($Ca^{2+}i$) from human rbcs was evaluated. The concentration of cAMP increased by 31% in the presence of MST7, and by 77% in the presence of MST7 and CTZ (phosphodiesterase 3 inhibitor), whereas the incubation with CTZ alone had no effect (Fig. 3A). This means that phosphodiesterase 3 endogenous activity was able to partially limit MST7 induced increases of [cAMP].

To test the involvement of MST7-dependent increases in cAMP on ATP release, we examined the effects of the PKA inhibitor H-89 on ATPe kinetics. Cells were pre-incubated for 5 min with 10 μM H-89 and ATPe kinetics was monitored upon MST7 addition (not shown). Under the present experimental conditions, H-89 inhibited ΔATP_{20} by 47 % (Fig. 3B).

Exposure of rbcs to MST7 did not affect [Ca^{2+}i] (Fig. 3C).

3.5. Cell adhesion and cAMP as potential modulators of ATP release in rbcs from humans and dogs

We have shown above in Fig. 1 that in human rbcs MST7 promoted release of ATP required cell adhesion, and that elevated [ATPe] correlated with an increase in [cAMP] (Fig. 4B). To evaluate the role of cAMP we also performed experiments in dog rbcs, which were reported not to exhibit cAMP dependent induction of ATP release [9].

Similarly to human rbcs, exposure of dog erythrocytes to MST7 produced no effects on non-adhered cells, whereas in adhered cells an acute 12-fold increase of [ATPe] was found (Fig. 4A). Dog rbcs treated with MST7 showed a slight [cAMP] increase, but such change was not significant. A correlation plot depicts the changes in cAMP and ATPe concentrations from dog and human rbcs in the absence (basal levels) or presence of 10 μM MST7 (Fig. 4B). Compared to dog rbcs, human rbcs showed a higher response to MST7 for both parameters assessed.

3.6. EctoATPase activity from human rbcs

Using suspensions of intact human rbcs, the rate of ATP hydrolysis was determined by following the time course of [^{32}P]Pi accumulation released from [γ-^{32}P]ATP (150–900 nM) (Fig. 5A). The rate of ATPe hydrolysis was not affected by MST7 exposure of cells. EctoATPase activity was calculated both, as the initial rate of [^{32}P]Pi accumulation (estimated from Fig. 5A) of cell suspensions, or alternatively as the initial rate of ATPe extinction monitored by real-time luminometry using non-adhered cells (data not shown). EctoATPase activity followed a linear function with ATP concentrations over an ample range (Fig. 5B).

3.7. Conduits of ATP release in human and mice rbcs

We previously reported that pannexin 1 inhibitors reduced ATP release from rbcs exposed to a cAMP generating cocktail [3]. Therefore, the possibility that pharmacological inhibition of pnx by CBX and PBC may inhibit MST7 induced ATP release of human rbcs was investigated.

Cells pre-incubation with 10 μM or 100 μM CBX, 10 μM PBC, or 10 μM of both CBX and PBC caused a 2–5 fold reduction in the initial rate of [ATPe] increase, and almost complete inhibition of the slower increase late phase (Fig. 6A).

Consequently, ΔATP_{20} values were reduced 47–52% with CBX (10 and 100 μM) or PBC (10 μM), and 68% with 10 μM CBX + 10 μM PBC. No significant differences in ΔATP_{20} values were found among the different blockers and concentrations (Fig. 6B).

To investigate further the role of pnx on ATP release from human rbcs, key experiments were repeated using rbcs from $pnx^{+/+}$ and $pnx^{-/-}$ mice exposed to either MST7 or the cAMP-activating cocktail 3V (a cAMP activating cocktail containing 10 μM isoproterenol, 30 μM forskolin and 100 μM papaverine).

We previously reported that in human rbcs the increase of [ATPe] induced by 3V (Fig. 10) was fully blocked by 10 μM CBX [3]. Similarly, in $pnx^{+/+}$ mice rbcs exposed to 3V, an acute induction of ATPe accumulation occurred that was fully blocked by CBX. On the contrary, in rbcs from $pnx^{-/-}$ mice, 3V was unable to increase [ATPe] from basal values (Fig. 7A).

MST7 exposure of $pnx^{+/+}$ mice rbcs caused an acute 5-fold increase of [ATPe] to a constant value. An activation of ATPe accumulation was also observed in rbcs from $pnx^{-/-}$ mice, but absolute levels were reduced by 57% when compared with control $pnx^{+/+}$ values (Fig. 7B). In $pnx^{+/+}$ mice rbcs, pre-incubation with either 10 μM CBX, 10 μM PBC or 10 μM CBX + 10μM PBC reduced MST7 dependent [ATPe] levels by 63–75% (Fig 8A). Absolute [ATPe] values (estimated as ΔATP_5) in the presence of these blockers were similar to that obtained using rbcs from $pnx^{-/-}$ mice (Fig 8B). Blockers had no effect on [ATPe] of MST7 exposed rbcs from $pnx^{-/-}$ mice (Fig. 8C and D).

Finally, the response to MST7 was analyzed using rbcs from $pnx^{+/+}$, $pnx^{+/-}$ and $pnx^{-/-}$ mice. When compared to $pnx^{+/+}$ rbcs, ΔATP_5 was 62% in $pnx^{+/-}$ mice rbcs and 43% in $pnx^{-/-}$ mice rbcs, though differences between cells from $pnx^{+/-}$ and $pnx^{+/+}$ mice were not significant (Fig. 9).

3.8. Effect of 3V on MST7-ATPe release from non-adhered human rbcs

Experiments in Fig. 10 were designed to check if MST7, when used with 3V as a co-stimulus, would be able to stimulate ATP release in the absence of cell adhesion. The cocktail 3V was previously optimized to induce an acute cAMP-dependent ATP release in human rbcs [3]. Unlike in the case of MST7, 3V effect on ATPe kinetics was similar in the absence or presence of cell adhesion (Fig. 10A and B).

When non-adhered cells were simultaneously stimulated with 3V and MST7, an acute and strong increase of [ATPe] was obtained to a maximal value at 3.4 ± 0.6 pmol/10^6 cells, which remained constant thereafter (Fig. 10A). Similar experiments performed in the presence of MST7 and either 10 μM isoproterenol or 30 μM forskolin (two components of 3V mixture) produced minor increases in [ATPe] (Fig. 10C).

3.9. Modeling ATPe kinetics of MST7 estimulated rbcs

Results of Figs. 2 and 5 showed that in human rbcs MST7 induced a slight cell swelling and a non-linear accumulation of ATPe, while at the same time cells displayed ectoATPase activity over a wide range of nanomolar concentrations. We next built a data-driven mathematical model to quantify how these processes control ATPe kinetics and to predict the kinetics of transmembrane ATP transport mediating ATP release.

3.9.1. Fluxes mediating ATP release—Exposure of human rbcs to 10 μM CBX induced a partial inhibition of ATPe kinetics (Fig. 6). This was interpreted in the model by assuming that ATP release (J_R) required two conduits (mediating subfluxes J_{R1} and J_{R2}), with one subflux (J_{R1}) being fully blocked by CBX (Fig. 11A).

Model fitting to experimental data allow simulating the kinetics of ATPe in the absence or presence of CBX with reasonable accuracy, and to predict the corresponding subfluxes mediating ATP transport (Appendix Fig. 1).

Following MST7 stimulation, J_R showed a steep, 1.5 x 10^4-fold increase from 0.044 to 668 nM/min in less than 1 sec, followed by a slow nonlinear decrease to a constant value of 1.3 nM/min. J_{R1} showed a high initial amplitude followed by a steep decay.

On the other hand J_{R2}, which acted as the only transport conduit in the presence of CBX, presented a different kinetics. It increased to a maximum only 18 of J_R, but since the decay rate was slow, after 40 sec J_{R2} was higher than J_{R1} (see inset to Fig 11B). Thus, J_{R2} became the main subflux of ATP release.

During MST7 exposure the rate of ATPe hydrolysis was very low compared to $J_{R.}$ Hence, the effect of ectoATPase activity on ATPe kinetics was negligible.

3.9.2. EctoATPase activity—During MST7 exposure the rate of ATPe hydrolysis was very low compared to $J_{R.}$ Thus, the effect of ectoATPase activity on ATPe kinetics is expected to be minor. Accordingly, when the best fitting curve of ATPe kinetics (which takes into account the measured ectoATPase activity) was compared to a predicted ATPe kinetics assuming full blockage of ectoATPase activity, the differences between both curves were almost negligible (Appendix Fig. 1 C). On the contrary, when a standard ectoATPase activity (about 43 times that of human rbcs, as observed in most cell types, [43]) is fed into the model, the predicted ATPe kinetics departed strongly from the best fitting curve, reflecting the potential importance of ATPe hydrolysis in controlling ATPe kinetics.

3.9.3. Cell volume—Experimental results showed that in a standard isosmotic medium MST7 induced cell swelling and ATP efflux. The resulting time-dependent ATPe accumulation was highly reduced when MST7 was used in a hyperosmotic medium where changes in cell volume were blocked (Fig. 2). Following model-dependent fit to these data the predicted fluxes under both experimental conditions (i.e., MST7 in isosmotic and hyperosmotic media) could be deduced. As compared to MST7 in isosmotic medium, in hyperosmotic medium the initial peak of ATP flux decreased 70% whereas the decay phase remained almost unaltered (Appendix Fig. 2 A and B).

Volume-dependent changes in ATPe kinetics might be due to a decrease in intracellular ATP concentration which, according to the model (Appendix, Eq. 3) is one of the main factors driving ATP efflux. Alternatively, cell volume may affect the permeability parameters of the conduits mediating ATP transport (see Appendix).

Since MST7 did not affect ATPi content (basal ATPi content was 192.4 ± 15.5 pmol/10^6 cells, and after 10 min of MST7 exposure it was 178.8 ± 10.8 pmol/10^6 cells), changes in [ATPi] should be inversely related to cell volume. However, when [ATPi] was allowed to decrease in the model as a function of cell volume enhancement, the predicted effects on ATPe kinetics were minor (Appendix Fig. 2 C). This means that MST7-dependent swelling affected ATPe kinetics mainly by controlling ATP permeability.

4. DISCUSSION

The main goal of this study was to identify the key factors controlling ATPe kinetics of human rbcs exposed to MST7. In addition to a quantitative analysis of the dynamic balance between ATP efflux and ATPe hydrolysis yielding a particular ATPe kinetics, we looked into potential modulators of ATPe release such as $Ca^{2+}i$, cAMP formation, cell adhesion and cell swelling.

4.1. Stimuli triggering ATP release

4.1.1. Cell adhesion—In standard off-line measurements of ATPe (11), experiments are usually performed with rbcs in suspensions at relatively high hematocrits to approach the *in vivo* condition where these cells occupy about 40% of blood volume. However, under this condition, to avoid their natural tendency to sediment, rbcs are subjected to mechanical forces due to medium agitation, stirring and/or collisions among cells. In a previous report we demonstrated that such forces can by themselves modulate the potency of other ATP release stimuli [3]. On the other hand, in real-time ATPe measurements used in the present study, cells remain quiescent on the bottom of the chamber during the experiment, with reagents added by diffusion and without medium exchange. Therefore, the present protocol minimized those external forces and allowed us to assess ATP release in a more controlled environment.

As a first approach we compared the response to MST7 recorded by ATPe off-line measurements that required holding rbcs in suspension, with data obtained by ATPe real-time measurements with quiescent rbcs.

Using rbcs suspensions at 20% hematocrit, exposure to MST7 induced a strong increase in [ATPe], thus corroborating previous reports [10, 16]. However, the magnitude of the response decreased with the hematocrit, so that MST7 activation was lost below 1% hematocrit. A tentative explanation would be that as the hematocrit decreases, cells in suspension are more diluted and therefore less prone to mechanical perturbations that may be required to trigger ATP release upon MST7 stimulation.

Similarly to the low hematocrit condition, in the online ATPe measurements where cells were held quiescent at the bottom of the chamber, MST7 did not alter [ATPe]. However, MST7 activated ATP release when cells were adhered to coverslips pre-coated with 0.001% poly-D-lysine. At such a very low concentration of poly-D-lysine (about 10 times lower than that used in most studies; [44]), negatively charged human rbcs adhered firmly to the positively-charged surface and remained discoidal in shape [45]. Interestingly, MST7-induced ATP release was also observed when cells were adhered to collagen- or laminin-coated coverslips, whereas addition of L-lysine or poly-D-lysine to assay medium containing non-adhered cells did not produce any response *per se*. Therefore, cell adhesion itself, but not the electric charge, may act as a pre-stimulus triggering MST7 activation of ATP efflux.

4.1.2. Cell volume—Another novel aspect of MST7 action on human rbcs is the induction of isosmotic swelling. Since a slightly hyposmotic medium caused similar increases in cell

volume as MST7 in isosmotic medium, and triggered the release of ATP (Suppl. Fig. 4), we hypothesized that swelling might be one of the components contributing to MST7-induced ATP release. Accordingly, when MST7 was added in a hyperosmotic medium that fully blocked cell swelling, the accumulation of ATPe was attenuated. Hence, small increases in cell volume, probably inducing mechanical forces on the cell surface, were able to positively modulate the effect of MST7 on ATP release from human rbcs.

In line with this idea, [ATPe] is enhanced by mechanical deformations when rabbit rbcs are forced to cross small filters [10] or when human rbcs transit along microfluidic channels [46].

Moreover, using off-line measurements at high hematocrits, MST7 activation of ATP release was blocked by *Bordetella pertussis* toxin, implying the involvement of a Gi-dependent mechanism of ATP release [10]. In our online setup system a similar incubation treatment with pertussis toxin produced 89 % inhibition of ATPe accumulation, suggesting that a second –though minor– Gi-independent mechanism of MST7 induced ATP release might be operative as well.

4.1.3. Intracellular signaling—During the past 15 years, experimental evidence extensively supported the role of cAMP as an important signal that triggers ATP release from human, rat, mouse and rabbit rbcs [9, 47, 48, 49], whereas potential effects of $Ca^{2+}{}_i$ have not been described. Dog erythrocytes were sometimes used as negative controls for the action of cAMP-dependent stimuli, since they appeared not to exhibit a pathway for cAMP-dependent ATP release [3, 9].

In the present study, exposure of human rbcs to MST7 did not change [Ca^{2+}i], but caused a small although significant increase in [cAMP]. Supporting the notion that PKA mediates cAMP-dependent ATP release, we showed that H-89, a potent inhibitor of PKA, attenuated MST7-induced ATPe accumulation.

On the other hand, in dog rbcs challenged with MST7, a trend towards increased [cAMP] was observed but such changes were not significant. In spite of this difference, and even when dog rbcs were reported not to release ATP in response to deformation, hypoxia, or by treatment with activators of adenylyl cyclases or cAMP analogs [9], these cells responded similarly to human rbcs in that non-adhered cells did not respond to MST7, whereas poly-D-lysine-adhered cells did respond with a significant increase in [ATPe].

Results discussed above indicate that, for quiescent rbcs, an increase in [cAMP] does not trigger ATP release unless cells are pre-activated by adhesion. But, is it possible to prime non adhered cells to respond to MST7?

In a previous report we demonstrated that a cAMP activating cocktail (so-called “3V”) containing isoproterenol (a β-adrenergic agonist), forskolin (an activator of adenylyl cyclases) and papaverine (a phosphosdiesterase inhibitor) strongly increased [cAMP] and triggered ATP release from human rbcs [3]. Unlike MST7, 3V did not alter cell volume, and induced the same ATPe kinetics in the absence or presence of cell adhesion. Interestingly, the simultaneous addition of 3V and MST7 to non-adhered cells produced a strong ATP

release, yielding a similar ATPe kinetics than that obtained by incubating adhered cells with MST7.

This cAMP "rescue" of MST7 effect may require a robust and persistent cAMP elevation since activation of adenylyl cyclase by β-adrenergic stimulation or forskolin, in the absence of phosphodiesterase inhibition produced only a slight change in [ATPe]. Thus, in quiescent human rbcs, either cell adhesion or the stimulation of cAMP synthesis by 3V is required for MST7 to induce ATP release.

4.2. ATP efflux and ATPe regulation

Exposure of human rbcs to MST7 led to a non-linear increase in [ATPe] (Fig. 1) until a steady level was achieved. EctoATPase activity, a potential consumer of ATPe, behaved strictly as a linear function of ATPe concentration and cell density (Fig. 5).

The specific ectoATPase activity was very low compared to other cell types, a feature shared by all non-nucleated mammalian rbcs [3, 43]. However, if assessed *in vivo* with 40% hematocrit this ATPe hydrolyzing activity of rbcs would consume ~6% of total plasma ATP per minute. It means that the contribution of ectoATPase activity from rbcs to total ATPe hydrolysis in blood is important (a feature neglected in most studies), because the low specific ectoATPase activity is compensated by the high abundance of rbcs in blood.

However, in our online measurements performed at low cell density, where the volume of 3 x 10^6 cells occupied less than 1% of total assay volume, the calculated ATPe consumption by ectoATPase activity was so low that time-dependent ATPe accumulation mainly reflected the kinetics of ATPe release.

Due to the absence of vesicles, conductive or transport mechanisms are responsible for rbcs ATP release. Among them, pannexin 1 has been postulated to form hexameric pores that allow or facilitate passive transport of ATP across the plasma membrane [50]. Pannexin 1-activity can be blocked by CBX or PBC [29] and channel activity consistent with pannexin 1 was recorded in membrane patches excised from human rbcs [51].

By assuming two conduits mediating ATP transmembrane transport, our mathematical model predicted the kinetics of the two corresponding partial fluxes.. A CBX-sensitive flux was rapidly activated and deactivated, whereas a CBX-resistant flux, smaller in magnitude than the other one, showed a rapid activation phase followed by a slow decay (Appendix Fig. 1 B). Clearly, during the first 40 sec of MST7 exposure, ATP release was mainly controlled by the CBX-sensitive flux, whereas the CBX-resistant flux became important beyond that time point. As shown in Appendix Fig. 1 A, the best fit model was compatible with a certain degree of interaction between the two conduits. This is because, according to the model, CBX not only blocked the CBX-sensitive flux, but was also capable of affecting the kinetic parameters of the CBX-resistant flux.

To better assess the role of pannexin 1 on ATP efflux, several experiments were repeated using rbcs from $pnx^{+/+}$ and $pnx^{-/-}$ mice. Two important features of MST7-induced ATPe kinetics were similar in rbcs from humans and mice: upon rbcs exposure to MST7, there is a

time-dependent steep increase in [ATPe] that could be partially inhibited by either CBX or PBC.

Provided CBX specifically inhibited pannexin 1, rbcs from $pnx^{-/-}$ mice should display similar ATPe kinetics than those of $pnx^{+/+}$ mice pre-incubated with CBX. This was indeed what we found (Fig. 8). Also, rbcs from $pnx^{-/-}$ reached MST7-induced ATPe levels similar to those of rbcs from $pnx^{+/+}$ mice pre-incubated with CBX, PBC, or CBX plus PBC. Importantly, none of these blockers altered [ATPe] of rbcs from $pnx^{-/-}$ mice. Similarly, a probenecid-tolerant release of ATP was also observed in rbcs from $pnx^{-/-}$ mice stimulated by a hypotonic K^+ solution [52].

Although these results do not solve the issue of whether pannexin 1 acts as a single conduit or as an essential component of a transport protein complex (as postulated by Silverman et al., [30]), they indicate that pannexin 1 is the major, if not the only CBX-sensitive pathway for ATP release from rbcs exposed to MST7 and to a cAMP activating cocktail. Moreover, most of the predicted initial 15,000-fold increase in ATP efflux required for MST7 dependent ATPe kinetics is due to activation of this CBX-sensitive pathway.

4.3. Erythrocytes from dogs and humans

Erythrocytes from dogs were used to validate the effect of cell adhesion on ATP efflux observed in human rbcs. Compared to human rbcs, dog rbcs displayed lower basal cAMP levels, and a modest, non-significant increase of cAMP concentration upon MST7 exposure. Despite these differences, in both species cell adhesion triggered MST7-induced ATP release (Figs 4), whereas in non-adhered dog and human rbcs [ATPe] did not change. This means that in rbcs from humans and dogs adhesion acts as a pre-stimulus potentiating MST7 induction of ATP release.

4.4. Testing the mathematical model

The model designed to explain ATPe kinetics (see Appendix) presents three key features:

1- at any time, [ATPe] is determined by the balance between the rates of ATP release and ATPe hydrolysis by ectoATPase activity;

2- two different conduits mediate the non-lytic release of ATP;

3- ATP transmembrane transport by these conduits is driven by the chemical gradient of ATP across the cell membrane, multiplied by a permeability term that accounts for the kinetics of ATP transport.

In principle, the ATP chemical gradient depends on the difference between [ATPi] and [ATPe]. In the current experimental conditions, the accumulated [ATPe] is in the nanomolar range and [ATPi] is in the milimolar range, leaving [ATPi] as the main thermodynamic parameter driving ATP efflux. Since our results showed that ATPi mass of cells did not vary during MST7 exposure, [ATPi] should decrease with cell swelling, causing a concomitant decrease of ATP release. However, in human rbcs, the observed change on [ATPi] had almost no effect on ATP release (Appendix Fig. 2 C). Conversely, model-dependent fit to

experimental ATPe kinetics allowed us to calculate the predicted ATP efflux in the absence of volume change (i.e., MST7 in hyperosmotic medium) or in its presence (i.e., MST7 in isosmotic medium), showing that changes in cell volume mostly modified the permeability parameters of ATP transport (see Fig. 2C in Appendix).

4.5. Speculations regarding the role of adhesive forces and the physiological context of ATPe homeostasis

The quantitative ATPe profile described for human rbcs in the present and in a previous study [3] is compatible with an *in vivo* scenario where, under non-stimulated conditions, [ATPe] is maintained constant at a relatively low value, and acute increases occur in response to certain physiological and/or pathological conditions.

Provided that in particular areas of the circulation the rates of ATPe hydrolysis by different ecto and exo nucleotidases of blood cells, the vascular endothelium and plasma are not high enough, and that paracrine distances from ATP exit are short, rbcs-derived ATPe would then interact with P2 receptors of the vascular endothelium. As a consequence, the production of endothelium-derived vasodilators will be stimulated, that will relax the smooth muscle cells lining the vessels and increase the vascular caliber. *In vivo* studies using rbcs from humans, rabbit and mice support the hypothesis that rbcs derived ATPe is an important determinant of blood flow [6, 49, 52].

It is in this physiological context that cell adhesion might constitute an important signal modulating ATP release (as observed in this study).

Adhesion of rbcs to other cells is reported to play key roles in various pathological processes including malarial parasite invasion and sickle cell sequestration, as well as in physiological processes such as cell senescence [53].

In the future, improved variants of MST7 could be used as pharmacological tools to enhance ATP release from rbcs. This can be particularly important in the treatment of patients with diseases such as hyperinsulinemia, type 2 diabetes and primary pulmonary hypertension among others, where the efflux of ATP in response to various physiological stimuli is highly diminished. Also, the ability of rbcs to release ATP declines upon a prolonged storage in the blood banks, and this phenomenon correlates with negative clinical outcomes for patients receiving transfusions of stored blood [54]. Moreover infective diseases like malaria are associated with vascular obstruction.

In all these situations, MST7 variants might be used with pharmacological purposes to help control the production of endothelium-derived vasodilators that mediate the relaxation of the smooth muscle cells lining the vessels and hence, to control the vascular caliber.

Supplementary Material

Refer to Web version on PubMed Central for supplementary material.

Acknowledgments

This work was supported by Consejo Nacional de Investigaciones Científicas y Técnicas (CONICET) Grant PIP 1187 and 112 20110100639, Secretaría de Ciencia y Técnica, Universidad de Buenos Aires Grant 20020100100090, and Agencia Nacional de Promoción Científica y Tecnológica Grant 0151 of Argentina. ERL was supported by NIH grant P01-HL-0343223.

We are grateful to Dr. Maria Marta Rivero (Hemolab, Canine Blood Bank, Buenos Aires) for providing healthy canine blood samples, Juliana Sesma for technical help, and Dr. MP. Faillace, for critical reading of the manuscript. We are specially grateful to Catherina van Heusden for her assistance on studies using pnx$^{-/-}$ mice.

MFLD is a CONICET doctoral fellowship holder. MVE, SVV, OP and PJS are career researchers from CONICET.

Abbreviations

ATPe	extracellular ATP
ATPi	intracellular ATP
CBX	carbenoxolone
CTZ	cilostazol
GEFs	guanine exchange factors
MST	mastoparan
PBC	probenecid
pnx	pannexin 1
pnx$^{+/+}$	pannexin 1 wild type mice
pnx$^{+/-}$	pannexin 1 heterozygous mice
pnx$^{-/-}$	pannexin 1 knockout mice, PTX, pertussis toxin
rbcs	red blood cells

References

1. Gorman MW, Feigl EO, Buffington CW. Human Plasma ATP Concentration. Clin Chem. 2007; 53:318–325. [PubMed: 17185366]
2. Lazarowski ER, Boucher RC, Harden K. Mechanisms of Release of Nucleotides and Integration of Their Action as P2X- and P2Y-Receptor Activating Molecules. Mol Pharmacol. 2003; 64:785–795. [PubMed: 14500734]
3. Montalbetti N, Leal Denis MF, Pignataro OP, Kobatake E, Lazarowski ER, Schwarzbaum PJ. Homeostasis of Extracellular ATP in Human Erythrocytes. J Biol Chem. 2011; 286:38397–38407. [PubMed: 21921036]
4. Sprague RS, Stephenson AH, Ellsworth ML. Red not dead: signaling in and from erythrocytes. Trends Endocrinol Metabol. 2007; 18:350–355.
5. González-Alonso J, Olsen DB, Saltin B. Erythrocyte and the Regulation of Human Skeletal Muscle Blood Flow and Oxygen Delivery. Cir Res. 2002; 91:1046–1055.
6. Sprague RS, Bowles EA, Achilleus D, Ellsworth ML. Erythrocytes as controllers of perfusion distribution in the microvasculature of skeletal muscle. Acta Physiol. 2011; 202:285–292.
7. Ellsworth ML, Sprague RS. Regulation of blood flow distribution in skeletal muscle: role of erythrocyte-released ATP. J Physiol. 2012; 590:4985–4991. [PubMed: 22586223]

8. Hellsten Y, Nyberg M, Mortensen SP. Contribution of intravascular versus interstitial purines and nitric oxide in the regulation of exercise hyperaemia in humans. J Physiol. 2012; 590:5015–5023. [PubMed: 22733661]
9. Sprague RS, Ellsworth ML, Stephenson AH, Lonigro AJ. Participation of cAMP in a signal-transduction pathway relating erythrocyte deformation to ATP release. Am J Physiol Cell Physiol. 2001; 281:C1158–C1164. [PubMed: 11546651]
10. Olearczyk JJ, Stephenson AH, Lonigro AJ, Sprague RS. Heterotrimeric G protein Gi is involved in a signal transduction pathway for ATP release from erythrocytes. Am J Physiol Heart Circ Physiol. 2004; 286:H940–H945. [PubMed: 14615280]
11. Sridharan M, Adderley SP, Bowles EA, Egan TM, Stephenson AH, Ellsworth ML, Sprague RS. Am J Physiol Heart Circ Physiol. 2010; 299:H1146–1152. [PubMed: 20622111]
12. Zimmerberg J, Parsegian VA. Polymer inaccessible volume changes during opening and closing of a voltage-dependent ionic channel. Nature. 1986; 323:36–39. [PubMed: 2427958]
13. Higashijima T, Burnier J, Ross EM. Regulation of Gi and G0 by Mastoparan, related amphiphilic peptides, and hydrophobic amines. J Biol Chem. 1990; 265:14176–14186. [PubMed: 2117607]
14. Park HS, Lee SY, Kim YH, Lee SJ, Choi MU. Membrane perturbation by mastoparan 7 elicits a broad alteration in lipid composition of L1210 cells. Biochim Biophys Acta. 2000; 1484:151–162. [PubMed: 10760465]
15. Sprague RS, Stephenson AH, Bowles EA, Stumpf MS, Lonigro AJ. Reduced Expression of Gi in Erythrocytes of Humans With Type 2 Diabetes Is Associated With Impairment of Both cAMP Generation and ATP Release. Diabetes. 2006; 55:3588–3593. [PubMed: 17130508]
16. Hanson MS, Stephenson AH, Bowles EA, Sprague RS. Insulin inhibits human erythrocyte cAMP accumulation and ATP release: role of phosphodiesterase 3 and phosphoinositide 3-kinase. Exp Biol Med. 2010; 235:256–262.
17. Dupré DJ, Robitaille M, Rebois RB, Hébert TE. The Role of Gβγ Subunits in the Organization, Assembly, and Function of GPCR Signaling Complexes. Annu Rev Pharmacol Toxicol. 2009; 49:31–56. [PubMed: 18834311]
18. Wang L, Olivecrona G, Götberg M, Olsson ML, Winzell MS, Erlinge D. ADP Acting on P2Y13 Receptors Is a Negative Feedback Pathway for ATP Release From Human Red Blood Cells. Circ Res. 2005; 96:189–196. [PubMed: 15604418]
19. Pafundo DE, Alvarez CL, Krumschnabel G, Schwarzbaum PJ. A Volume Regulatory Response Can Be Triggered by Nucleosides in Human Erythrocytes, a Perfect Osmometer No Longer. J Biol Chem. 2010; 285:6134–6144. [PubMed: 20040601]
20. Erlinge D, Burnstock G. P2 receptors in cardiovascular regulation and disease. Purinergic Signal. 2008; 4:1–20. [PubMed: 18368530]
21. Kunapuli SP, Daniel JL. P2 receptor subtypes in the cardiovascular system. Biochem J. 1998; 336:513–523. [PubMed: 9841859]
22. Burnstock G. Dual control of vascular tone and remodelling by ATP released from nerves and endothelial cells. Pharmacol Rep. 2008; 60:12–20. [PubMed: 18276981]
23. Ellsworth ML, Ellis CG, Goldman D, Stephenson AH, Dietrich HH, Sprague RS. Erythrocytes: Oxygen Sensors and Modulators of Vascular Tone. Physiology. 2009; 24:107–116. [PubMed: 19364913]
24. Crecelius AR, Kirby BS, Luckasen GJ, Larson DG, Dinenno FA. ATP-mediated vasodilatation occurs via activation of inwardly-rectifying potassium channels in humans. J Physiol. 2012; 590:5349–5359. [PubMed: 22777673]
25. Sévigny J, Sundberg C, Braun N, Guckelberger O, Csizmadia E, Qawi I, Imai M, Zimmermann H, Robson SC. Differential catalytic properties and vascular topography of murine nucleoside triphosphate diphosphohydrolase 1 (NTPDase1) and NTPDase2 have implications for thromboregulation. Blood. 2002; 99:2801–2809. [PubMed: 11929769]
26. Kukulski F, Lévesque SA, Lavoie EG, Lecka J, Bigonnesse F, Knowles AF, Robson SC, Kirley TL, Sévigny J. Comparative hydrolysis of P2 receptor agonists by NTPDases 1, 2, 3 and 8. Purinergic Signal. 2005; 1:193–204. [PubMed: 18404504]
27. Locovei S, Bao L, Dahl G. Pannexin 1 in erythrocytes: Function without a gap. Proc Natl Acad Sci USA. 2006; 103:7655–7659. [PubMed: 16682648]

28. Qiu F, Dahl G. A permeant regulating its permeation pore: inhibition of pannexin 1 channels by ATP. Am J Physiol Cell Physiol. 2009; 296:C250–C255. [PubMed: 18945939]
29. Ransford GA, Fregien N, Qiu F, Dahl G, Conner GE, Salathe M. Pannexin 1 Contributes to ATP Release in Airway Epithelia. Am J Respir Cell Mol Biol. 2009; 41:525–534. [PubMed: 19213873]
30. Silverman W, Locovei S, Dahl G. Probenecid, a gout remedy, inhibits pannexin 1 channels. Am J Physiol Cell Physiol. 2008; 295:C761–C767. [PubMed: 18596212]
31. Sridharan M, Sprague RS, Adderley SP, Bowles EA, Ellsworth ML, Stephenson AH. Diamide decreases deformability of rabbit erythrocytes and attenuates low oxygen tension-induced ATP release. Exp Biol Med. 2010; 235:1142–1148.
32. Sprague RS, Bowles EA, Achilleus D, Stephenson AH, Ellis CG, Ellsworth ML. A selective phosphodiesterase 3 inhibitor rescues low PO_2-induced ATP release from erythrocytes of humans with type 2 diabetes: implication for vascular control. Am J Physiol Heart. 2011; 301:H2466–H2472.
33. Thuet KM, Bowles EA, Ellsworth ML, Sprague RS, Stephenson AH. The Rho kinase inhibitor Y-27632 increases erythrocyte deformability and low oxygen tension-induced ATP release. Am J Physiol Heart. 2011; 301:H1891–H1896.
34. Seminario-Vidal L, Okada SF, Sesma JI, Kreda SM, van Heusden CA, Zhu Y, Jones LC, O'Neal WK, Penuela S, Laird DW, Boucher RC, Lazarowski ER. Rho signaling regulates Pannexin 1-mediated ATP release from airway epithelia. J Biol Chem. 2011; 286:26277–26286. [PubMed: 21606493]
35. Strehler BL. Bioluminescence assay: principles and practice. Methods Biochem Anal. 1968; 16:99–181. [PubMed: 4385967]
36. Brown, AM. ATP and ATPase determination in red blood cells. In: Ellory, JC.; Young, JD., editors. Red Cell Membranes - A Methodological Approach. Academic Press; London: 1982. p. 223-238.
37. Pafundo DE, Chara O, Faillace MP, Krumschnabel G, Schwarzbaum PJ. Kinetics of ATP and cell velume regulation of hyposmotically challenged goldfish hapatocytes. Am J Physiol Regul Integr Comp Physiol. 2008; 294:R220–R233. [PubMed: 17928510]
38. Gorman MW, Marble DR, Ogimoto K, Feigl EO. Measurements of adenine nucleotides in plasma. Luminescence. 2003; 18:173–181. [PubMed: 12701093]
39. Kwant WO, Seeman P. The erythrocyte ghost is a perfect osmometer. J Gen Physiol. 1970; 55:208–219. [PubMed: 5413078]
40. Grynkiewicz G, Poenie M, Tsien RY. New Generation of Ca^{2+} Indicators with Greatly Improved Fluorescence Properties. J Biol Chem. 1985; 260:3440–3450. [PubMed: 3838314]
41. Schwarzbaum PJ, Kaufman SB, Rossi RC, Garrahan PJ. An unexpected effect of ATP on the ratio between activity and phosphoenzyme level of Na^+/K^+-ATPase in steady state. Biochim Biophys Acta. 1995; 1233:33–40. [PubMed: 7833347]
42. Vázquez A, Tudela J, Varón R, García-Cánovas F. Determination of hemoglobin through its peroxidase activity on chlorpromazine. J Biochem Biophys Meth. 1991; 23:45–52. [PubMed: 1918800]
43. Bencic DC, Yates TJ, Ingermann RL. Ecto-ATPase Activity of Vertebrate Blood Cells. Physiological Zool. 1997; 70:621–630.
44. Freshney, RI. Culture of Animal Cells: A Manual of Basic Technique. 5. Wiley and sons; New York: 2005.
45. Hategan A, Sengupta K, Kahn S, Sackmann E, Discher DE. Topographical Pattern Dynamics in Passive Adhesion of Cell Membranes. Biophys J. 2004; 87:3547–3560. [PubMed: 15339814]
46. Forsyth AM, Wan J, Owrutsky PD, Abkarian M, Stone AH. Multiscale approach to link red blood cell dynamics, shear viscosity, and ATP release. Proc Natl Acad Sci USA. 2011; 108:10986–10991. [PubMed: 21690355]
47. Jagger JE, Bateman RM, Ellsworth ML, Ellis CG. Role of erythrocyte in regulating local O_2 delivery mediated by hemoglobin oxygenation. Am J Physiol Heart Circ Physiol. 2001; 280:H2833–H2839. [PubMed: 11356642]
48. Ellsworth ML. Red Blood Cell–Derived ATP as a Regulator of Skeletal Muscle Perfusion. Med Sci Sport Exer. 2004:35–41.

49. Sprague RS, Hanson MS, Achilleus D, Bowles EA, Stephenson AH, Sridharan M, Adderley S, Ellsworth ML. Rabbit Erythrocytes Release ATP and Dilate Skeletal Muscle Arterioles in the Presence of Reduced Oxygen Tension. Pharmacol Rep. 2009; 61:183–190. [PubMed: 19307706]
50. Dubyak GR. Both sides now: multiple interactions of ATP with pannexin-1 hemichannels. Focus on “A permeant regulating its permeation pore: inhibition of pannexin 1 channels by ATP”. Am J Physiol Cell Physiol. 2009; 296:C235–C241. [PubMed: 19179656]
51. Locovei S, Wang J, Dahl G. Activation of pannexin 1 channels by ATP through P2Y receptors and by cytoplasmic calcium. FEBS Lett. 2006; 580:239–244. [PubMed: 16364313]
52. Qiu F, Wang J, Spray DC, Scemes E, Dahl G. Two non-vesicular ATP release pathways in the mouse erythrocyte membrane. FEBS Lett. 2011; 585:3430–3435. [PubMed: 21983290]
53. Oldenborg PA, Zheleznyak A, Fang YF, Lagenaur CF, Gresham HD, Lindberg FP. Role of CD47 as a Marker of Self on Red Blood Cells. Science. 2000; 288:2051–2054. [PubMed: 10856220]
54. Zhu H, Zennadi R, Xu BX, Eu JP, Torok JA, Telen MJ, McMahon TJ. Impaired adenosine-5′-triphosphate release from red blood cells promotes their adhesion to endothelial cells: A mechanism of hypoxemia after transfusion. Crit Care Med. 2011; 39:2478–2486. [PubMed: 21765360]
55. Sabirov RZ, Okada Y. ATP release via anion channels. Purinergic Signal. 2005; 1:311–328. [PubMed: 18404516]
56. Kaji DM. Effect of membrane potential on K-Cl transport in human erythrocytes. Am J Physiol Cell Physiol. 1993; 264:C376–C382.
57. Akaike H. Data analysis by statistical models. No To Hattatsu. 1992; 24:127–133. [PubMed: 1567644]
58. Hoops S, Sahle S, Gauges R, Lee C, Pahle J, Simus N, Singhal M, Xu L, Mendes P, Kummer U. COPASI - a COmplex PAthway SImulator. Bioinformatics. 2006; 22:3067–3074. [PubMed: 17032683]

Appendix. Modeling of ATPe kinetics of MST7 challenged rbcs

A simple mathematical model was built to account for the experimentally observed ATPe kinetics when human erythrocytes were incubated with 10 μM MST7.

In the model, [ATPe] is controlled by the rate of non-lytic ATP release (J_R), which accounts for one or more mechanisms allowing ATP efflux in the absence of lysis, and the rate of ATPe consumption by ectoATPase activity (J_V).

Time dependent changes in [ATPe] are given by

$$\frac{d[ATP_e]}{dt} = J_R - J_V \quad \text{Eq. 1}$$

where J_R and J_V are the fluxes of ATP release and of ATPe hydrolysis, respectively.

The rate of ATPe consumption (J_V)

A linear expression for the dependence of J_V on ATPe concentration was derived empirically after analyzing data of ectoATPase activity assayed in intact human erythrocytes suspended in assay medium over an ample range of ATPe concentrations (100–900 nM; see Fig. 5):

$$J_V = k_{ATP} \cdot [ATP_e] \quad \text{Eq. 2}$$

Given that MST7 did not affect ectoATPase activity (Fig. 5), k_{ATP} was assumed to be constant throughout the experiment, both in the absence and presence of MST7.

Non-lytic release of ATP (J_R)

In human rbcs exposed to MST7, ATP release occurs in the absence of lysis and can thus be explained by one or more transport mechanisms. Efflux of ATP is assumed to be mediated by passive, facilitated diffusion as:

$$J_R = P\underbrace{\left(\left[ATPi\right]-\left[ATPe\right]\right)}_{\text{chemical gradient}}$$

Eq. 3

where P denotes a permeability term (whose properties are explained below), and [ATPi] and [ATPe] are the intracellular and extracellular ATP concentrations, respectively.

As it stands, J_R depends on "P" multiplied by the chemical gradient of ATP across the cell membrane. The electrical ATP gradient, on the other hand, can be calculated as "z. F. Vm" (where z denotes the electrical charge of ATP, F is the Faraday constant and Vm the membrane electrical potential). However, even considering that at intracellular pH=7.2 the electric charge of ATP (a weighted average of all anionic ATP species; see [54]) lies around −2.4, due to the relative low membrane potential of human rbcs (about −10 mV, [56]) the electrical ATP gradient represents about 1% of total ATP electrochemical gradient, and was therefore not considered in Eq. 3.

Since changes in [ATPe] occur in the nanomolar range whereas [ATPi] is millimolar (see Results) the chemical gradient is approximately equal to [ATPi].

The permeability term of Equation 3

The non-linear accumulation of [ATPe] observed in MST7 stimulated erythrocytes (Fig. 1A) can be interpreted by assuming time dependent changes in the flux of ATP release (J_R). The model assumes that changes in J_R are due to different degrees of activation of the conduits responsible for ATP efflux. Accordingly, in the unstimulated condition, there is a basal, isosmotic, stationary state of flux (i). Exposure to MST7 induces an irreversible transition to a stimulated state (s) followed by a subsequent irreversible decay to a final state (f). For any given ATP conduit this transition is formulated as the following irreversible process:

where k_1 and k_2 are first order rate constants that govern the kinetics of this transition. The fraction of conduit molecules in the initial, stimulated and final states, denoted as x_i, x_s and x_f, respectively, vary with time according to the following differential mass law equations:

$$\begin{aligned}\frac{dx_i}{dt}&=-k_1\cdot x_i\\ \frac{dx_s}{dt}&=k_1\cdot x_i-k_2\cdot x_s\\ \frac{dx_f}{dt}&=k_2\cdot x_s\end{aligned}\quad \text{Eq. 4}$$

Values of x vary from 0 to 1 and at every time are related by:

$$x_i+x_s+x_f=1 \quad \text{Eq. 5}$$

The permeability P in Eq. 3 is given by

$$P=x_i\cdot p_i+x_s\cdot p_s+x_f\cdot p_f \quad \text{Eq. 6}$$

so that J_R can be now expressed as:

$$J_R=(x_i\cdot p_i+x_s\cdot p_s+x_f\cdot p_f)\cdot([ATP_i]-[ATP_e]) \quad \text{Eq. 7}$$

where p_i, p_s and p_f are the permeability parameters of the initial, stimulated and final conduit states, respectively. Since the values of these parameters do not change with time, and the chemical gradient only varies slightly during MST7 induction (see below), the time course of J_R is mainly controlled by the time dependence of x_i, x_s and x_f.

In the case of two conduits undergoing a similar two step transition (i.e., i → s → f, as in Scheme 1), with each flux being driven by the same chemical gradient (i.e, $[ATP_i]$-$[ATP_e]$), J_R can be expressed as the sum of two fluxes, with each flux exhibiting their corresponding permeability parameters where both P_1 and P_2 are described by:

$$J_R=J_{R1}+J_{R2}=(P_1+P_2)\cdot([ATP_i]-[ATP_e]) \quad \text{Eq. 8}$$

$$P_1=x_{i1}\cdot p_{i1}+x_{s1}\cdot p_{s1}+x_{f1}\cdot x_{f1} \quad \text{Eq. 9}$$

$$P_2=x_{i2}\cdot p_{i2}+x_{s2}\cdot p_{s2}+x_{f2}\cdot x_{f2} \quad \text{Eq. 10}$$

Prior to MST7 exposure,

$$x_i^0=1 \quad x_s^0=x_f^0=0 \quad \text{Eq. 11}$$

so that initial permeabilities for each conduit are given by p_i (p_{i1} and p_{i2}).

Before exposure to MST7, basal ATP release (i.e, J_R in the absence of MST7) is assumed to be balanced by ectoATPase activity (J_v), so that [ATPe] remains steady in the unstimulated condition.

To simulate the transition induced by MST7, k1 in Eq. 4 is fixed at zero until the stimulus is applied.

The final state is given by:

$$x_i^{\infty}=x_s^{\infty}=0 \quad x_f^{\infty}=1 \quad \text{Eq. 12}$$

and thus the permeability parameter for $t \rightarrow \infty$ is p_f.

Fitting of models to experimental data

Model dependent fits were applied to the experimentally obtained ATPe kinetics, with the restriction that suitable models should be able to fit simultaneously to profiles of ATPe accumulation in the absence and presence of carbenoxolone.

We considered a two conduit model accounting for J_{R1} and J_{R2} of Eq. 8, where carbenoxolone completely prevents the activation of J_{R1} (i.e., $k_{11}=0$). As shown in Appendix Fig. 1 A, assuming that both conduits are fully independent yields a poor fit (dotted lines in inset of Appendix Fig. 1 A). According to the Akaike criterion [57], a much better fit was attained by assuming a certain degree of interaction between both pathways (continuous lines in inset of Appendix Fig. 1). Particularly, it was considered that carbenoxolone not only blocked J_{R1} activation but also affected the values of parameters k_{22} and ps_2 of Eq 4 and 10.

Effects of cell swelling on ATP chemical gradient

To account for changes in cell volume induced by MST7, [ATPi] can be decomposed as

$$[ATP_i]=\frac{mATP_i}{Vt} \quad \text{Eq. 13}$$

with mATPi being the intracellular mass of ATP, and Vt the average cell volume of erythrocytes at different time points during the experiment. Since MST7 exposure of rbcs did not vary mATPi, this magnitude was considered constant.

The fluorometric technique used for volumetric experiments quantified time dependent changes in relative cell volume (Vr; Fig. 2A)

$$Vr=\frac{Vt}{V0} \quad \text{Eq. 14}$$

where volume at time 0 is one (V0) and volume changes at different times (Vt) are related to this value.

Considering Eqs. 3, 13 and 14, J_R can now be expressed as

$$J_R = P\left(\frac{mATP_i}{V0 \cdot Vr} - [ATP_e]\right) \quad \text{Eq. 15}$$

In this equation, values of Vr at any time were obtained by fitting a biexponential function to the experimentally observed changes in Vr (Fig. 2A).

Predictions of the model to assess the importance of ectoATPase activity

The best fitting model was used to predict the relative importance of ectoATPase activity on ATPe kinetics. Predictions were made by assuming either $k_{ATP} = 0$ (i.e., blockage of ectoATPase activity) or $k_{ATP} = 0.051\ min^{-1}$ (about 43 times the k_{ATP} derived from Fig. 5).

Model fitting

Best fitting values for the parameters, their associated standard errors, and all simulations shown in Results were numerically obtained with Copasi software, version 4.7 [58]. The Copasi file describing the model is available upon request.

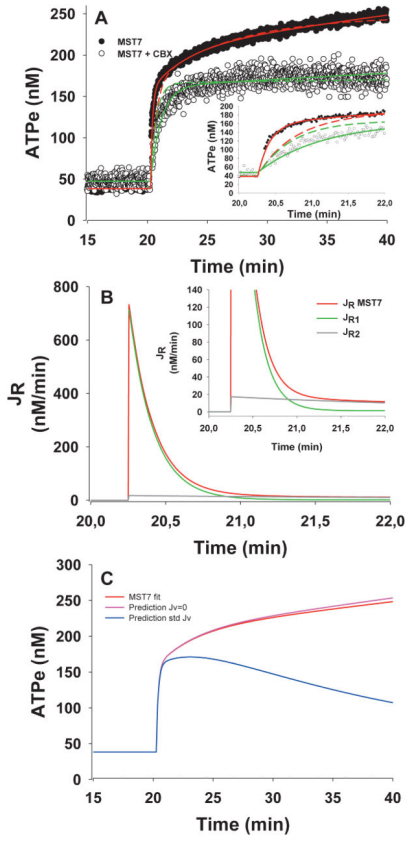

Appendix Figure 1.

Model fit to experimental ATPe kinetics in the presence of MST7 and predictions of the corresponding ATP fluxes.

A: The model (Equations 1–12 in Appendix) was fitted to the experimental MST7-dependent ATPe kinetics measured in the absence (red lines) or in the presence of 10 μM carbenoxolone (CBX, green lines). Dotted lines represent fitting of the model

where two fully independent ATP conduits were assumed, whereas the continuous lines represent a condition where a certain degree of interaction between the ATP conduits was allowed (as explained in Appendix). *Inset*: detail of the main graph from 20 to 22 min.

B: After achieving the best fit of the model to experimental data (continuous lines in A), the model predicted the total flux accounting for ATP release (J_R, in nM/min) and the partial fluxes which are either sensitive to CBX (J_{R1}) or resistant to CBX (J_{R2}). The inset shows a detail of the lower range of J_R values.

C: Prediction on the role of ectoATPase activity (J_v) on ATPe kinetics. Red line represents the best fit curve of the model to the experimental ATPe kinetics (taken from A). The pink line represents the predicted ATPe kinetics assuming full blockage of J_v. The blue line represents a predicted ATPe kinetics assuming 43-fold higher ectoATPase activity (std Jv) than the experimentally observed.

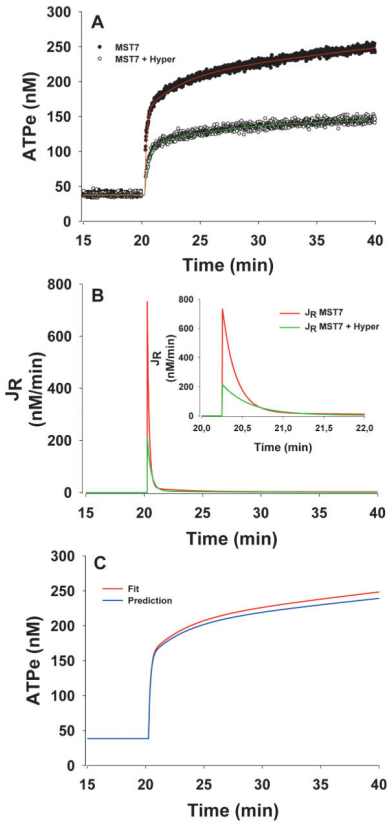

Appendix Figure 2.

Model fit to experimental ATPe kinetics from human rbcs in the presence of MST7 under isosmotic and hyperosmotic conditions. Predictions of the corresponding ATP fluxes.

A: Experimental data (taken from Fig. 2B) show the observed ATPe kinetics for cells exposed to MST7 in isosmotic medium (MST7) and in hyperosmotic medium (MST7+Hyper). Next, the model of Equations 1–12 (Appendix) was fitted to both conditions, with best fit values of the parameters given in Appendix Table 1. The lines represent the best fit model.

B: After achieving the best fit of the model to experimental data (lines in A), the corresponding fluxes could be predicted for MST7 exposed cell in isosmotic medium (red line; J_R MST7) and in hyperosmotic medium (green line; J_R MST7+Hyper). The inset shows a detail of data from main graph during the first minutes post stimulus.

C: Effect of cell volume on ATPe kinetics. The red line represents the best fit of the model to ATPe kinetics (similar to A). The blue line represents a prediction where changes in cell volume are allowed to affect ATP efflux, thereby affecting ATPe

kinetics. This was done considering the experimental changes in cell volume caused by MST 7 (Fig. 2A), and using Eq. 15 (see Appendix) to account for cell volume effects on J_{NL}.

Appendix Table 1

Parameters of the model

	MST7	MST7+CBX	MST7 Hyper
k_{11} (s^{-1})	6.2 ± 0.4	0	3.01 ± 0.06
k_{22} (s^{-1})	0.32 ± 0.02	1.13 ± 0.02	0.14 ± 0.01
p_{s1}/k_{21} (10^7)	58 ± 6	(*)	(**)
p_{s2}/k_{22} (10^7)	262 ± 5	560 ± 2	187 ± 13
$p_{f\,total}$ ($10^8\ s^{-1}$)	111 ± 3	(*)	11 ± 6
p_{f2} ($10^8\ s^{-1}$)	50 ± 2	(*)	(***)
p_{i2} ($10^8\ s^{-1}$)	2.24 ± 0.01	2.76 ± 0.01	2.17 ± 0.05
$p_{e1}/k_{21} \cdot p_{e2}/k_{22} \cdot 1/p_{f2}$	-	-	0.013 ± 0.008
k_{21} (s^{-1})	1000	(*)	(*)
k_{12} (s^{-1})	1000	(*)	(*)

Results are values of the best fit obtained by fitting the model to experimental data.

(*) Values provided by simultaneous fitting to the data obtained in isosmotic media (Iso) with or without CBX.

(**) This parameter was poorly defined by the fitting to the data obtained in hyperosmotic media (Hyper); it was computed from the better defined value of pe1/k21. pe2/k22. 1/pf2.

(***) Given that this value was poorly defined by the data it was computed from the value of the ratio pf total/pf2 obtained under isosmotic conditions.

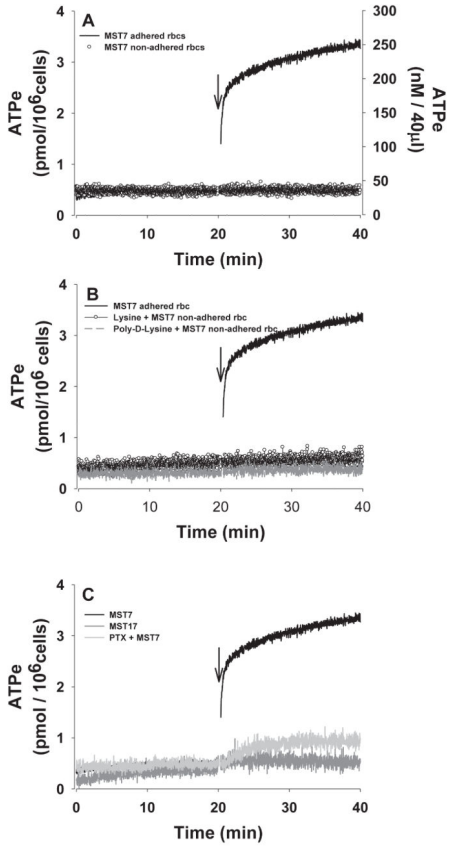

Figure 1. ATPe kinetics of MST7-exposed human rbcs

A: Effect of rbcs adhesion on ATPe kinetics. Rbcs were attached to coverslips coated with 0.001% poly-D-lysine (adhered cells), or loaded on the coverslip surface in the absence of any adherent substrate (non-adhered cells). The arrow indicates addition of 10 µM MST7.

B: Effect of lysine and poly-D-lysine on ATPe kinetics. Non-adhered rbcs were incubated in media containing either 67 mg/ml soluble L-lysine (N=2, n=4) or 0.01 mg/ml poly-D-lysine (N=2, n=4). Adhered rbcs were assayed using poly-D-lysine coated coverslips (as in Fig. 1A) (N=5, n=11). The arrow indicates addition of 10 µM MST7.

C: Effect of pertussis toxin (PTX) and MST17 on ATPe kinetics. Adhered rbcs were exposed to MST7, or pre-incubated 4 h with PTX (100 ng/mL) before MST7 exposure (N=3, n=5). In separate experiments, cells were exposed to MST17 (N=3, n=4), an inactive analog of MST7. The arrow indicates addition of 10 µM of either MST7 or MST17.

The time course of [ATPe] (pmol/10^6 cells and/or nM/40 µl) was quantified by real-time luminometry, as described in Materials and Methods.

Numbers of determinations (n) from independent preparations (N) are indicated.

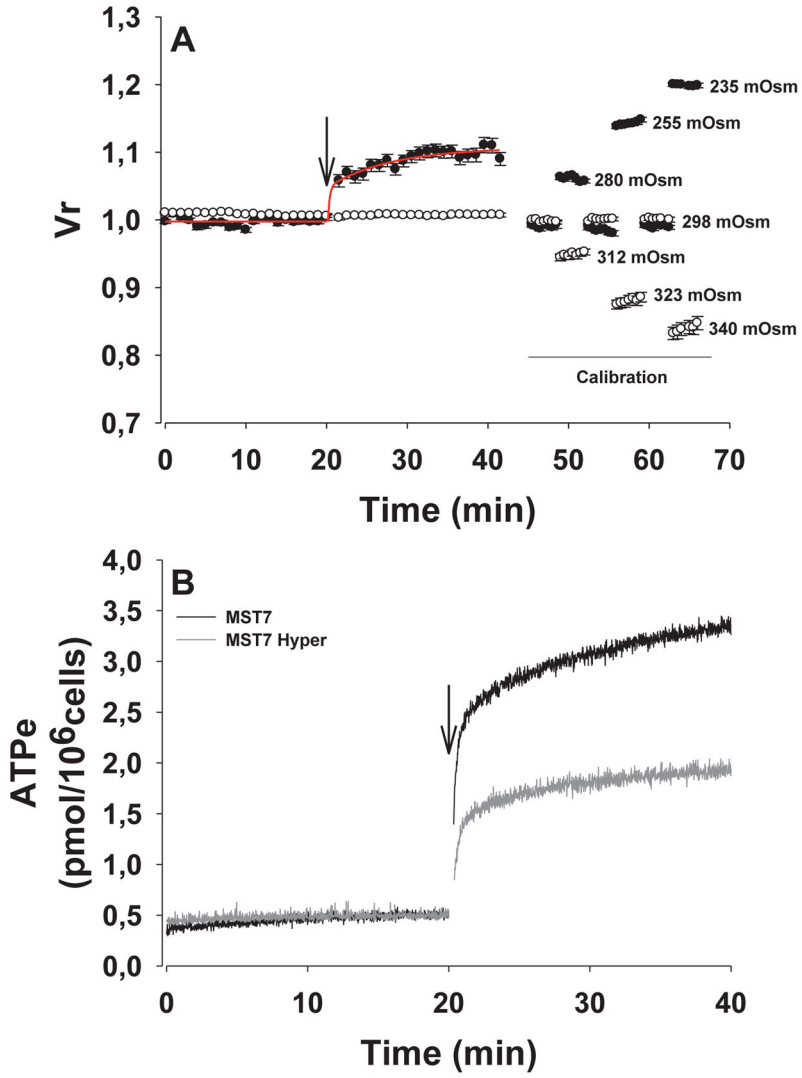

Figure 2. Effect of rbcs volume on ATPe kinetics of MST7 exposed human rbcs

A: Time course of relative cell volume (Vr) of human rbcs exposed to MST7. Rbcs were incubated in 200 µl of isosmotic medium (298 mosM) and after 20 min cells were exposed to 10 µM MST7 in isosmotic medium (●) or in hyperosmotic medium (345 mosM; ○). Calibration was performed at the end of each experiment by sequentially exposing rbcs to assay media with the following osmolarities (in mosM) 298, 280, 255 and 235 or 312, 323 and 340. Results are the mean ± SE of 20–30 rbcs (N=8) for isosmotic medium and 30–40 rbcs (N=4) for hyperosmotic medium. The red line represents fitting of a biexponential function to experimental data.

B: Effect of hyperosmotic medium on ATPe kinetics. Rbcs were attached to 0.001% poly-D-lysine-coated coverslips and stimulated with 10 µM MST7 in isosmotic medium (298 mosM; MST7) or hyperosmotic medium (345 mosM; MST7 Hyper) (N=3, n=5). The arrow indicates the exposure to stimuli.

Numbers of determinations (n) from independent preparations (N) are indicated.

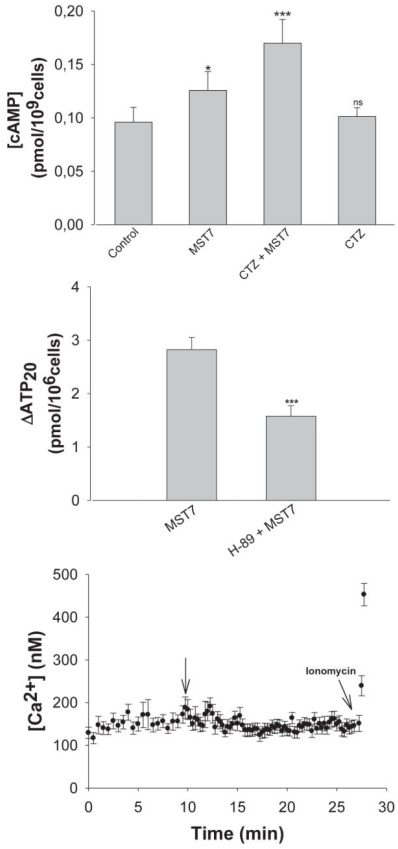

Figure 3. Second messengers and intracellular signaling

A: Levels of cAMP from human rbcs exposed to MST7. Rbcs were incubated for 10 min at room temperature under control conditions (Ctrl), or in the presence of either 10 μM MST7, 100 μM cilostazol (CTZ) + 10 μM MST7, or 100 μM CTZ. Results are means ± SEM (n=22, N=5) (*, $p<0.05$, ***, $p<0.001$, ns: non- significant *versus* control). The concentration of cAMP was determined by radio immunoassay using iodinated cyclic AMP-TME (see Materials and Methods).

B: Effects of the PKA inhibitor H-89 on [ATPe]. Adhered rbcs were exposed to 10 μM MST7 in cells pre-exposed for 5 min to vehicle (MST7) or to 10 μM H-89 (H-89 + MST7) (N=5, n=7). Values of [ATPe] are expressed as ΔATP_{20}, i.e., the difference between [ATPe] at 20 min post stimulus and basal [ATPe]. Results are means ± SEM. (***, $p<0.001$). Numbers of determinations (n) from independent preparations (N) are indicated.

C: Effect of MST7 on cytosolic free calcium concentration ($[Ca^{2+}i]$). Time-dependent changes in $[Ca^{2+}i]$ were assessed continuously by fluorescence microscopy using Fluo4-loaded rbcs. The arrow indicates addition of 10 μM MST7. At the end of each experiment, the signal was calibrated in the presence of ionomycin by adding 0.5 mM EGTA (to obtain minimal fluorescence intensity) or 2 mM $CaCl_2$ (to obtain maximal fluorescence intensity). Results are means ± SE of 20–30 rbcs (N=4).

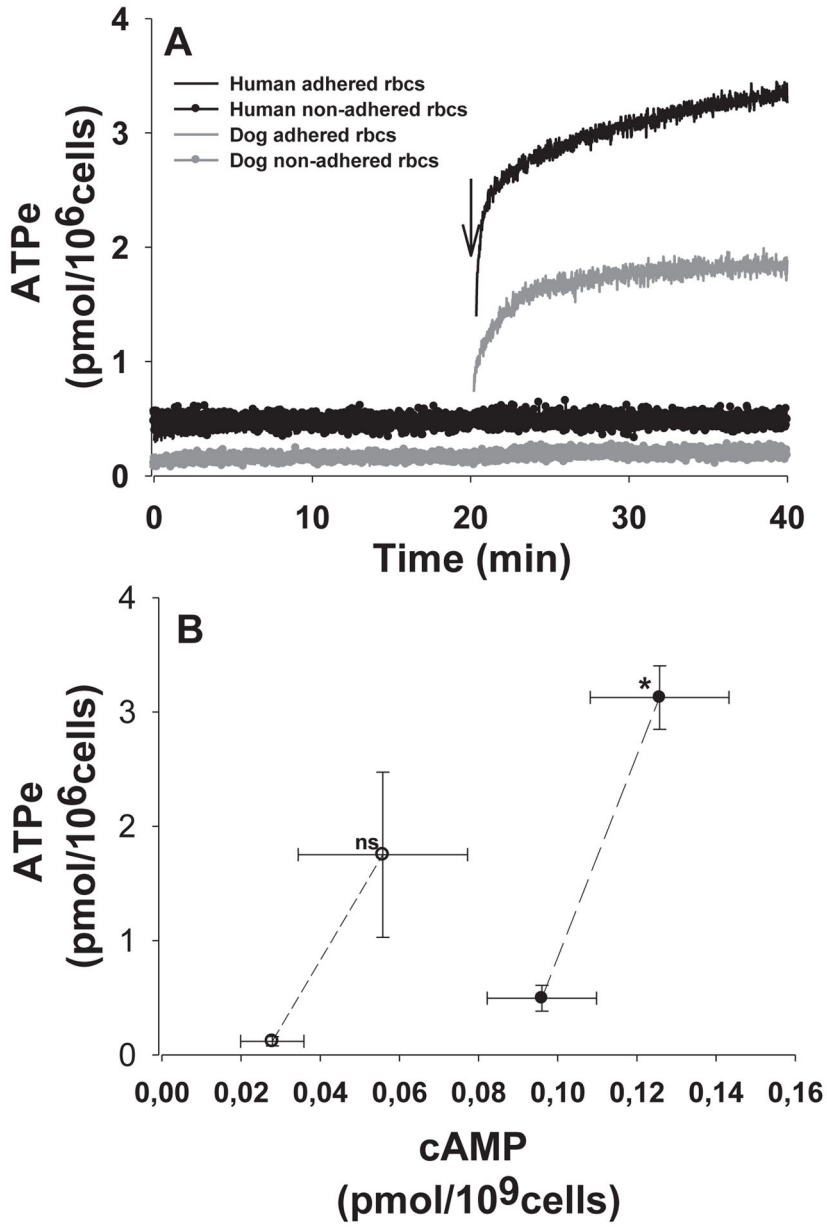

Figure 4. Cell adhesion and cAMP as potential modulators of ATP release in vertebrate rbcs

A: ATPe kinetics of adhered and non-adhered human and dog rbcs. Human and dog rbcs were attached to 0.001% poly-D-lysine-coated coverslips (adhered cells) or loaded on the coverslip surface in the absence of any adherent substrate (non-adhered cells). The arrow indicates addition of 10 μM MST7.

B: Correlation plot between [ATPe] and [cAMP] of rbcs from human (●) and dog (○). The concentrations of ATPe and cAMP were measured before (lower values) and after a 10 min exposure to 10 μM MST7. Results are means ± SE. (*, $p<0.05$ and ns: non-significant).

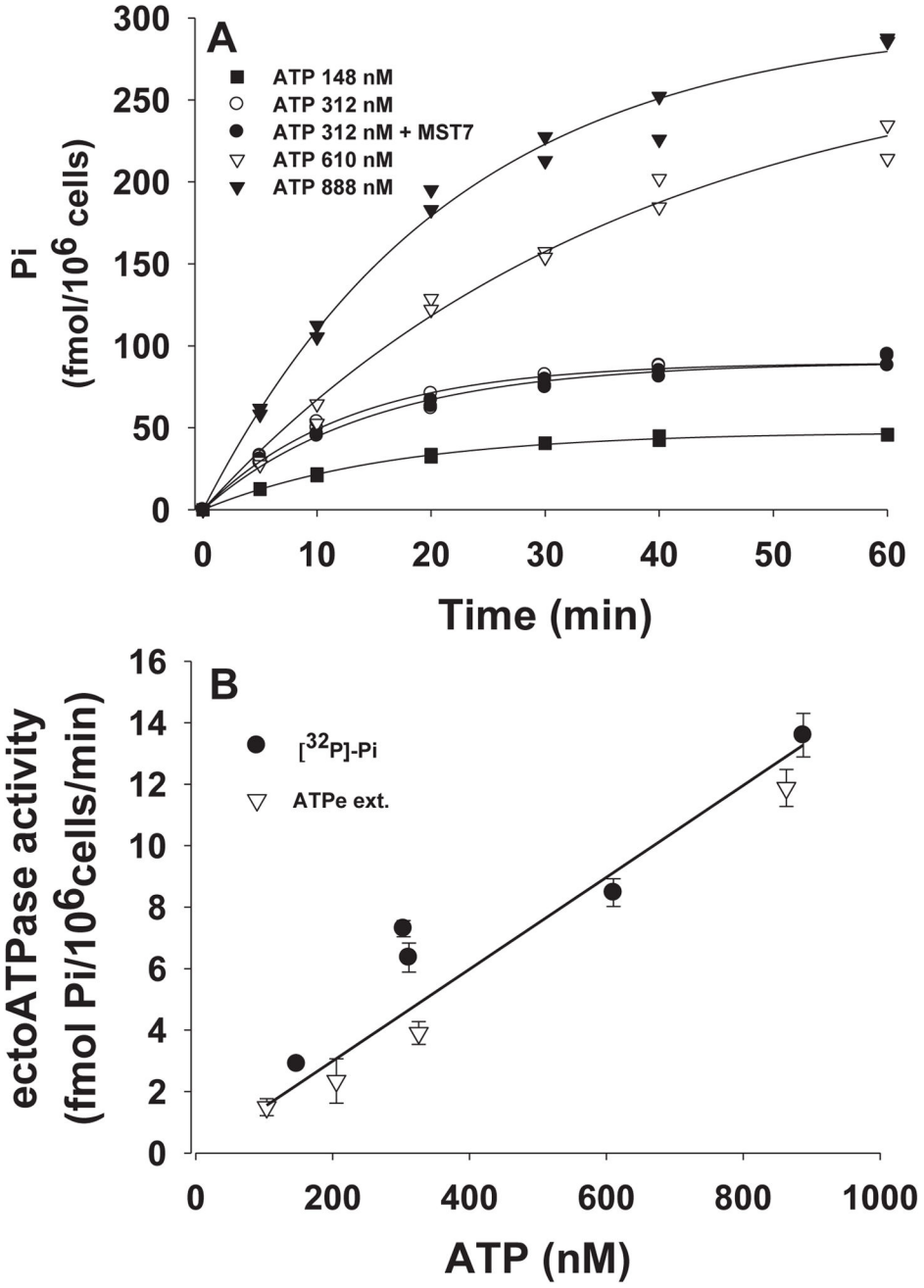

Figure 5. EctoATPase activity of intact human rbcs

A: The rate of ATPe hydrolysis was determined by following the accumulation of [^{32}P]Pi released from exogenous [γ-^{32}P]ATP (148–888 nM) added to a rbcs suspension at 20 % hematocrit. At ATP 312 nM the assays were performed in absence or presence of MST7. Results are expressed as Pi content and are means ± SEM. N=2, n=2 (fmol/10^6 cells). The continuous lines represent fitting of an exponential function to experimental data.

B: EctoATPase activity as function of [ATPe]. Close circles represent the initial rate of Pi accumulation ([^{32}P]Pi) obtained from experimental data of A. The open triangles represent the initial rate of ATPe extinction (ATPe ext.) in non-adhered rbcs incubated with ATP (100, 200, 320 and 860 nM) and monitored by real-time luminometry. Results are means ± SEM. The continuous line represents fitting of a linear function to experimental data.

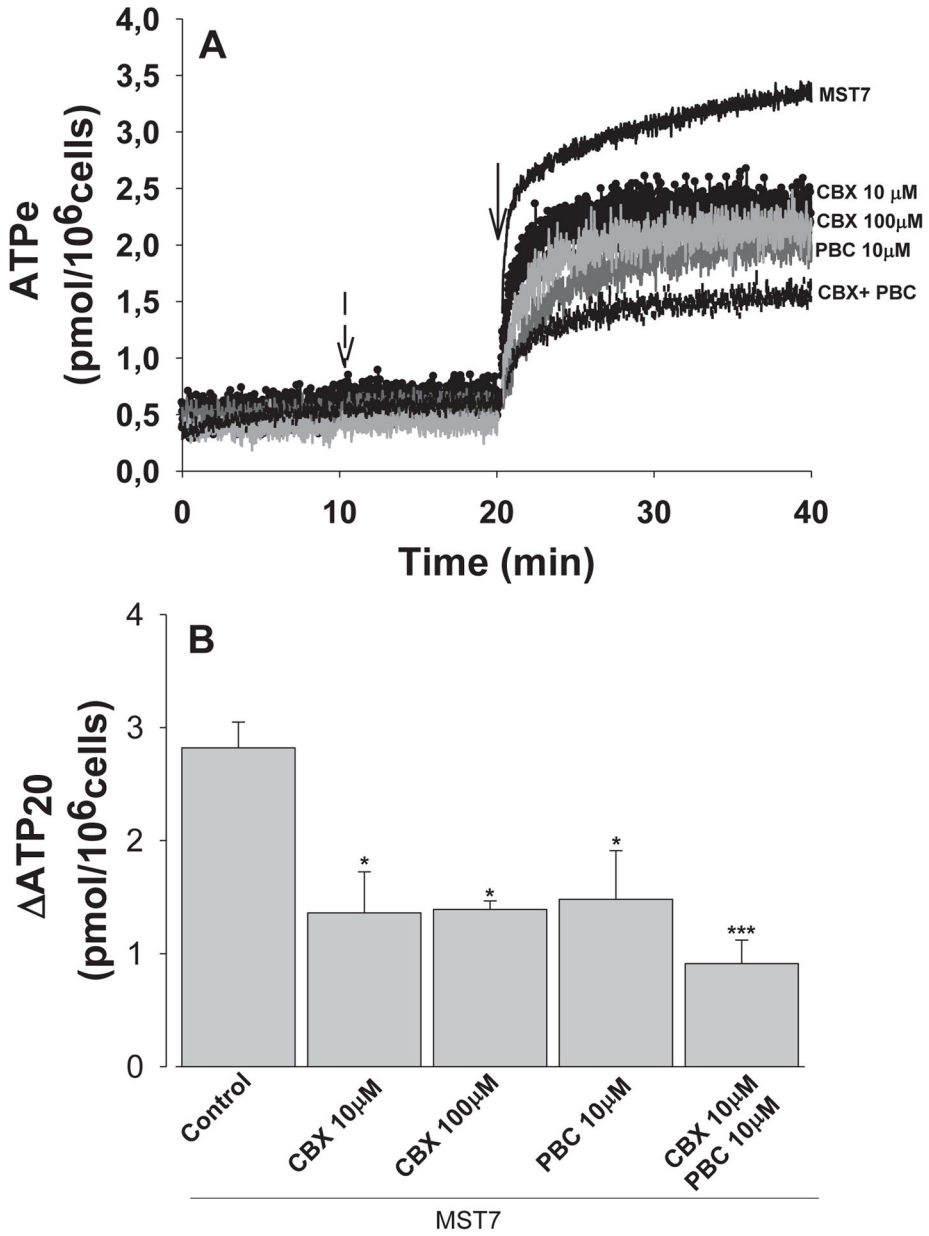

Figure 6. Conduits of ATP release in human rbcs

A: MST7-dependent ATPe kinetics of rbcs pre-incubated with blockers of ATP release. Prior to MST7 exposure, rbcs were adhered on 0.001% poly-D-lysine-coated coverslips and pre-incubated for 10 min with 10 or 100 μM carbenoxolone (CBX), 10 μM probenecid (PBC), or 10 μM of both CBX and PBC. The dotted arrow indicates addition of blockers and the full arrow indicates exposure to 10 μM MST7.

B: MST7-dependent increase of [ATPe] in the absence or presence of the different blockers and calculated from data shown in A. Values are expressed as ΔATP_{20}, i.e., the difference between [ATPe] at 20 min post stimulus and basal [ATPe]. Results are means ± SEM. (*, $p<0.05$, ***, $p<0.001$ *versus* MST7 alone).

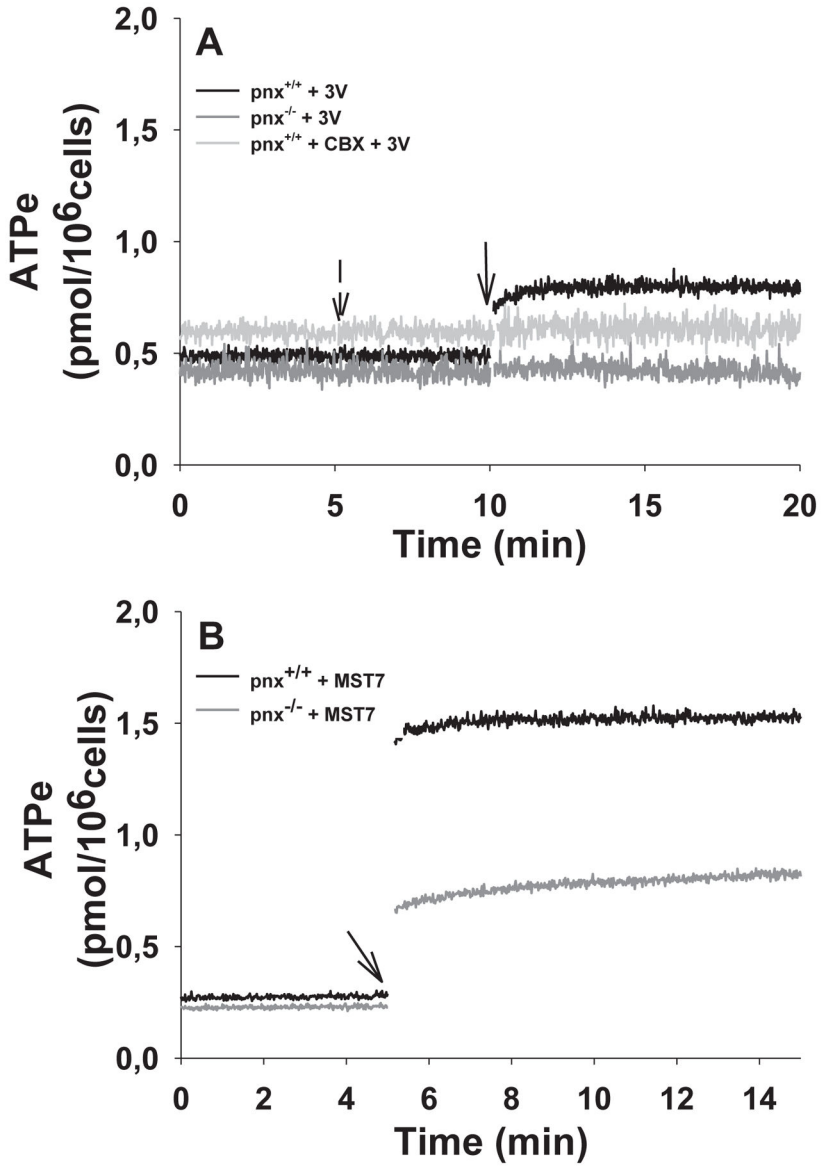

Figure 7. ATP release in mice rbcs

A: Effects of 3V on ATPe kinetics of rbcs from pnx $^{+/+}$ and pnx $^{-/-}$ mice. Rbcs adhered on 0.001% poly-D-lysine-coated coverslips were stimulated with 3V (10 μM isoproterenol, 30 μM forskolin and 100 μM) in the absence or presence of 10 μM CBX. The dotted arrow indicates addition of CBX and full arrow indicates addition of 3V.

B: Effects of MST7 on ATPe kinetics of rbcs from pnx $^{+/+}$ and pnx $^{-/-}$ mice. Rbcs adhered on 0.001% poly-D-lysine-coated coverslips were exposed to 10 μM MST7. The arrow indicates exposure to the stimulus.

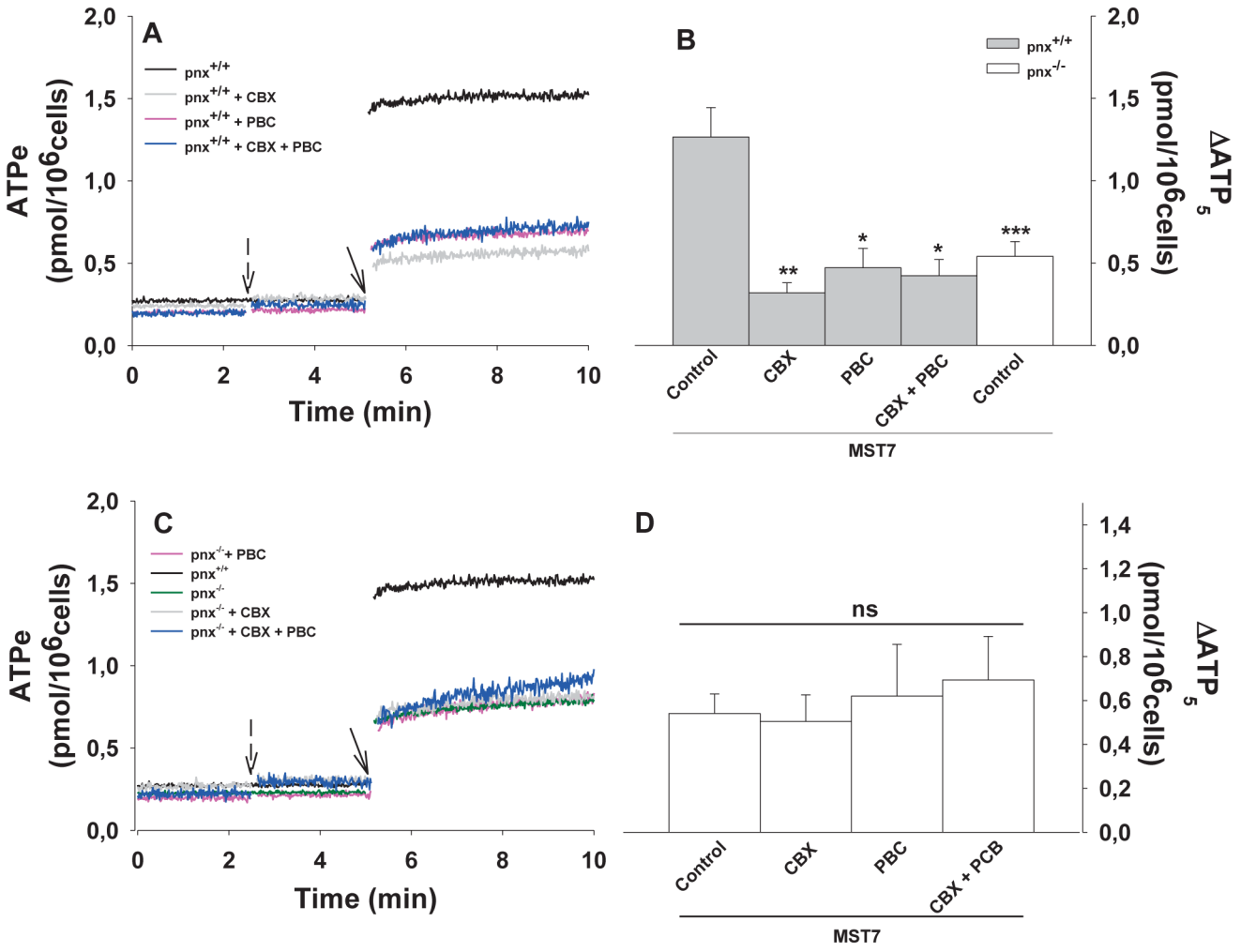

Figure 8. Conduits of ATP release in mice rbcs

A: ATPe kinetics of rbcs from pnx$^{+/+}$ mice pre-incubated with ATP release blockers. Rbcs adhered on 0.001% poly-D-lysine-coated coverslips were pre-incubated with 10 μM CBX, 10 μM PBC, or 10 μM of both CBX and PBC prior to 10 μM MST7 exposure. The dotted arrow indicates addition of blockers and the full arrow indicates addition of MST7.

B: MST7 dependent increases in [ATPe] in the absence or presence of the different blockers and calculated from data shown in A. Values are expressed as ΔATP_5, i.e., the difference between [ATPe] at 5 min post stimulus and basal [ATPe]. The value of ΔATP_5 of rbcs from pnx$^{-/-}$ mice exposed to MST7 is shown as a white bar. Results are means ± SEM. (*, $p<0.05$, **, $p<0.01$, ***, $p<0.001$ *versus* pnx$^{+/+}$ exposed to MST7).

C: ATPe kinetics of rbcs from pnx $^{-/-}$ mice pre-incubated with ATP release blockers. Rbcs adhered on 0.001% poly-D-lysine-coated coverslips were treated as in A. ATPe kinetics of rbcs from pnx$^{+/+}$ mice (taken from A) is also shown. The dotted arrow indicates addition of blockers and the full arrow indicates addition of 10 μM MST7.

D: MST7 dependent increases in [ATPe] in the absence or presence of the different blockers calculated from data of C. Values are expressed as ΔATP_5, i.e., the difference between [ATPe] at 5 min post stimulus and basal [ATPe]. Results are means ± SEM. (ns: non-significant *versus* MST7 alone).

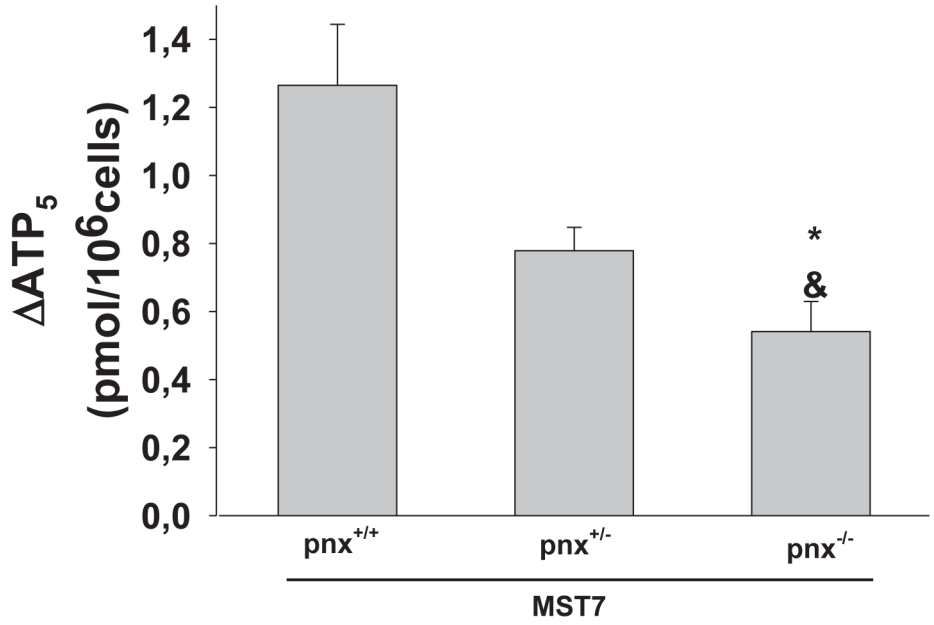

Figure 9. MST7 activation of ATP release in rbcs from pnx$^{+/+}$, pnx$^{+/-}$ and pnx$^{-/-}$mice

Cells adhered to 0.001% poly-D-lysine-coated coverslips were exposed to 10 μM MST7. Increases in [ATPe] were evaluated as the difference between [ATPe] at 5 min post stimulus and basal [ATPe], and are indicated as ΔATP_5. Results are means ± SEM. (* $p<0.001$ *versus* pnx$^{+/+}$ and & $p<0.05$ *versus* pnx$^{+/-}$).

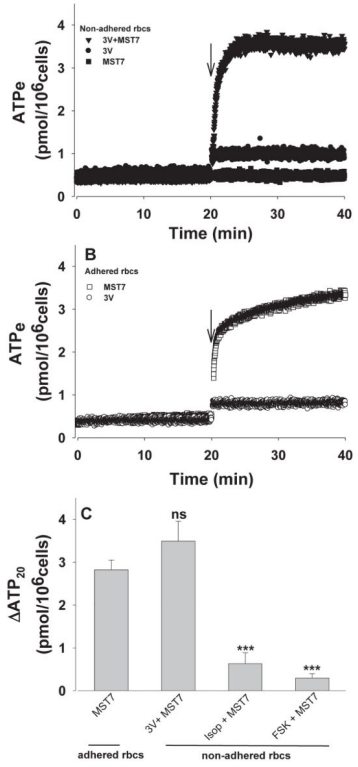

Figure 10. Effect of 3V on MST7-dependent ATPe release

A: ATPe kinetics of non- adhered human rbcs exposed to 3V, MST7 and MST7+ 3V. Rbcs were loaded on the coverslip surface in the absence of any adherent substance (non-adhered cells) and exposed to 3V, 10 μM MST7 or 10 μM MST7 + 3V. The arrow indicates exposure to stimuli.

B: ATPe kinetics of adhered rbcs exposed to 3V and MST7. Rbcs were adhered to 0.001% poly-D-lysine-coated coverslips (adhered cells) and exposed to 3V or 10 μM MST7. The arrow indicates the exposure to stimulus.

C: Release of [ATPe] induced by different stimuli. Adhered rbcs were exposed to MST7. Non-adhered rbcs were exposed to MST7 in presence of 3V, 10 μM isoproterenol (Isop) or 30 μM forskolin (FSK). Increases in [ATPe] are expressed as ΔATP_{20}, i.e., the difference between [ATPe] at 20 min post stimulus and basal [ATPe]. Results are means ± SEM. (***, $p<0.001$ and ns: non-significant *versus* adhered MST7 exposed rbcs).

Scheme 1.